One-bit quantization is good for programmable coding metasurfaces

Ya Shuang, Hanting Zhao, Menglin Wei, Qiang Cheng, Shi Jin, Tiejun Cui, Philipp del Hougne, Lianlin Li

SCIENCE CHINA
Information Sciences

• RESEARCH PAPER •

One-bit quantization is good for programmable coding metasurfaces

Ya SHUANG †[1], Hanting ZHAO †[1], Menglin WEI[1], Qiang CHENG[2,3,4], Shi JIN[2,3,4], Tie Jun CUI[2,3,4], Philipp HOUGNE[5] & Lianlin LI[6]

[1]*State Key Laboratory of Advanced Optical Communication Systems and Networks,Department of Electronics, Beijing,*100871,*China;*
[2]*Institute of Electromagnetic Space,Southeast University,Nanjing,*210096,*China;*
[3]*State Key Laboratory of Millimeter Waves, Southeast University, Nanjing,*210096,*China;*
[4]*Pazhou Laboratory,Guangzhou,*510330,*China;*
[5]*Univ Rennes,CNRS,IETR-UMR 6164,Rennes,*F-35000,*France*

Abstract The information-carrying programmable metasurfaces has found widespread applications in communication, sensing, and other related areas. However, there is a fundamental but unresolved problem, i.e., the rigorous understanding of the quantization of metasurface coding. Here, we theoretically investigate the performance difference between one-bit and continuous information-encoding metasurfaces. To this end, we derive analytical representations of system responses in various cases (single-input single-output, single-input multiple-output, and multiple-input multiple-output). We analyze the impact of one-bit coding (in contrast to continuous coding) in terms of the resulting channel cross-talk and reduction of information capacity in various representative scenarios from wireless communication and holography. Our main finding indicates that the one-bit coding yields a satisfactory performance in most practical scenarios; we also show that in many cases there are smart ways to mildly relax optimization constraints in order to reduce the performance gap between the one-bit and continuous coding. We expect that our results can provide theoretical guidance for a large variety of metasurface-assisted information systems for electromagnetic waves and other wave phenomena.

Keywords metasurfaces, metamaterials, information capacity, signal representation, one-bit coding metasurface

Citation Shuang Y, Zhao H T, Wei M L, et al.. One-bit quantization is good for programmable coding metasurfaces. Sci China Inf Sci, for review

1 Introduction

The ability to manipulate information-carrying electromagnetic (EM) fields pivotally underpins wireless communication, imaging and sensing, wireless power transfer, and other related areas. It has received long-standing interests in fundamental sciences, engineering and military contexts. Modern information systems typically rely on massive antenna arrays in combining with beamforming techniques to simultaneously improve the range of wireless link and reduce unwanted interference [1–4]. However, the bulky, costly and power-hungry hardware increasingly struggles to meet the requirements of ever-increasing amounts of connection nodes, especially with the advent of "green" Internet of Thing (IoT). An emerging alternative paradigm for EM wave manipulation is using programmable coding metasurfaces [5, 6], which are composed of ultrathin and inexpensive arrays of in-situ reprogrammable meta-atoms. The programmable coding metasurface has become an emerging member of a large family of metasurfaces holding large technological promise owing to their ability to manipulate the EM waves in a flexible manner. Initially, the programmable metasurfaces were designed to serve on the transmit side in combination with a carefully deployed source antenna [5, 7–12], as an alternative to the low-cost phased array antennas for beam forming in free space. Generally, they can be understood as a multi-port device linking various

* Corresponding author (email: tjcui@seu.edu.cn, philipp.delhougne@gmail.com, lianlin.li@pku.edu.com)
† Shuang Y and Zhao H T have the same contribution to this work.

input channels (sources) to various output channels (receivers) in an adaptive manner in terms of geometrical (number and location) and physical (signal response) port properties. Moreover, the programmable metasurfaces can be integrated into the propagation environment itself [13], as an alternative relaying mechanism in (quasi) free space [14–17] to optimize the available channels in scattering environments [18] or to conceive unconventional backscatter communication protocols [19, 20].

To date, many practical realizations of the programmable metasurfaces rely on one-bit (or fewbit) coding in order to further reduce the system cost, complexity and energy consumption. A onebit meta-atom is controlled with an externally applied one-bit voltage, and correspondingly has two distinct response states denoted by ' 0 ' and ' 1 '. For instance, upon illumination with a plane wave, the state ' 0 ' (' 1 ') may correspond to a reflection phase of $0°$ ($180°$). Given the success of one-bit coding in diverse applications including wireless communications, imaging and sensing [21–29], wireless power transfer [30, 31], programmable holography [32] and analog computing [33], a fundamental question [34, 35] arises: what is the achievable information capacity of a programmable metasurface built with one-bit coding meta-atoms (Reflection coefficient $R = \pm 1$) compared to the ideal case of continuously tunable meta-atoms ($R = A\exp(j\varphi)$ with the amplitude $|A| \leqslant 1$ and $0 \leqslant \varphi < 2\pi$) ? Interestingly, related questions about the impact of quantization on focusing (but not on programmable information encoding) has already arisen in related but distinct areas of wave engineering such as diffractive optical and acoustic elements (e.g. Fresnel lenses) [36–38], time reversal [39] and optical wavefront shaping in the complex media [40]. Very recently, the impact of the programmable metasurface quantization has received attention from a signal-processing perspective for the simplest case of single-input single-output (SISO) scenarios, in which the metasurface serves as an alternative relaying mechanism without encoding any information [41–44].

To comprehensively explore the quantization affects for information-encoding programmable metasurfaces operating in (quasi) free space, here we firstly derive the mathematical representations of the one-bit coding system response for three representative scenarios: SISO, single-input multiple-output (SIMO), and multiple-input multiple-output (MIMO). These scenarios link one or multiple input channels to one or multiple output channels. Our analysis reveals that the one-bit quantization gives rise to undesirable effects like energy leakage, parasitic unwanted beams, and channel cross-talk. We also find that in many practical applications the performance deterioration is negligible and can be limited under mild constraint relaxations. Then, we derive analytical expressions for the signal interferences and the reduction in channel capacity. Moreover, we illustrate our theoretical findings with concrete examples of programmable holography and wireless communications. We expect that our results can provide valuable guidance for the designs of the current and future metasurface-assisted EM information systems in wireless communications and sensing, as well as for various applications at other frequencies [45–52].

2 Representation of system response in one-bit coding metasurface

To start, we derive the system response of one-bit programmable coding metasurface acting as a reprogrammable wireless multi-port device that links various incident beams (from sources) to various outgoing beams (to receivers). To avoid complications due to the EM coupling effects, we group several adjacent meta-atoms together to form a "macro meta-atom". We then assume that the metasurface shown in Figure 1 is composed of $M \times N$ macro meta-atoms that can be modeled as having mutually independent EM responses. For convenience, we refer to the "macro meta-atom" as meta-atom hereafter.

2.1 Case I: SISO

For SISO, the one-bit coding metasurface is used to establish a wireless channel linking a source at $\boldsymbol{r}_s$ with an intended receiver at $\boldsymbol{r}_q$, as shown in Fig. 1a. This wireless link is easily established by suitably programming the metasurface. We assume that the signal power level of the source is $\mathcal{P}$; and the signal is desired to acquire a phase ϕ_q ($0 \leqslant \phi_q < 2\pi$) when it reaches $\boldsymbol{r}_q$ in a phase shift keying (PSK) scheme. We emphasize that, throughout this work, the information is not encoded by the source at $\boldsymbol{r}_s$ but through the modulation of EM wave by the metasurface. However, the scenario of information being encoded by the source is a special case of our model, where only the intensity of the radiation beam is concerned. A closed-form estimate of a suitable one-bit coding pattern of the metasurface for this purpose is $\mathcal{C}_{m,n}^{SISO} = \text{sign}\left[\cos\left(\tilde{\phi}_{nm}^{\text{SISO}}\right)\right]$,where $\tilde{\phi}_{nm}^{\text{SISO}} \equiv \tilde{\phi}_{m,n}(\boldsymbol{r}_q;\boldsymbol{r}_s)$ and $\tilde{\phi}_{m,n}(\boldsymbol{r}_q;\boldsymbol{r}_s) = \Delta_{m,n}(\boldsymbol{r}_q;\boldsymbol{r}_s) +$

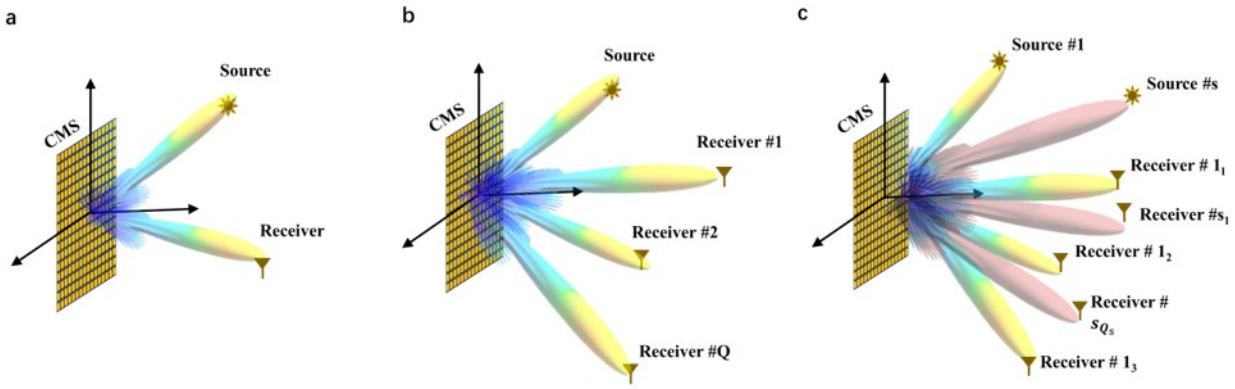

Figure 1 Fig. 1. Illustration of how a programmable coding-metasurface (CMS) acts as a wireless multiple-port device. a) SISO: CMS serves as a wireless ultrathin device with one input port and one output port, linking one source to one intended receiver. b) SIMO: CMS serves as a single-input multiple-output wireless device, connecting one source with $Q(Q>1)$ intended receivers (Receiver #1, Receiver #2, ..., Receiver #Q). c) MIMO: CMS serves as a wireless ultrathin device with S input ports and $\sum_{i=1}^{S} Q_i$ output ports. Each source (e.g., Source #s, $s=1,2,\ldots,S$) is linked to Q_i intended receivers (i.e., Receiver #s s_1, Receiver #s,. . ., Receiver #s_{Q_s}) by CMS.

$\phi(\boldsymbol{r}_q), \Delta_{m,n}(\boldsymbol{r}_q;\boldsymbol{r}_s) = k(\underbrace{|\boldsymbol{r}_s-\boldsymbol{r}_{m,n}|}_{R_{nm}(\boldsymbol{r}_s)} + \underbrace{|\boldsymbol{r}_q-\boldsymbol{r}_{m,n}|}_{R_{nm}(\boldsymbol{r}_q)})$. Herein, k denotes the wavenumber in free-space, and $\boldsymbol{r}_{m,n}$ denotes the location of metasurface element. Considering that the real location of the source $\mathbf{r}'$ is usually inaccurate or even unknown [19], we assume that the estimated location of the source is $\boldsymbol{r}_s$. Then, the response at $\mathbf{r}$ can be derived as (see details in Appendix A):

$$\widehat{\mathcal{H}}_{\text{SISO}}(\mathbf{r},\mathbf{r}';q,s) = \underbrace{E_1^{\text{SISO}}(\boldsymbol{r},\boldsymbol{r}';q,s)}_{\text{leading term}} + \underbrace{\sum_{p=-\infty,p\neq 1}^{\infty} B_p^{\text{SISO}} A_p^{\text{SISO}}(\boldsymbol{r},\boldsymbol{r}';q,s)\exp(jp\phi_q)}_{\text{perturbation terms}} \tag{1}$$

Herein, j is the imaginary unit and

$$E_1^{SISO}(\boldsymbol{r},\boldsymbol{r}';q,s) = B_1^{SISO} A_1^{SISO}(\boldsymbol{r},\boldsymbol{r}';q,s)\exp(j\phi_q)$$
$$A_p^{SISO}(\boldsymbol{r},\boldsymbol{r}';q,s) = \sum_{m,n} \frac{\exp\left[j\left(p\Delta_{nm}(\boldsymbol{r}_q;\boldsymbol{r}_s) - \Delta_{nm}(\boldsymbol{r};\boldsymbol{r}')\right)\right]}{R_{nm}(\boldsymbol{r})R_{nm}(\boldsymbol{r}')}$$

and $B_p^{\text{SISO}} = \begin{cases} -\frac{j^{p+1}}{\pi}\frac{2}{p}, & \text{if } p \text{ is odd} \\ 0, & \text{else} \end{cases}$. Note that $\left|B_1^{SISO}\right| = \left|B_{-1}^{SISO}\right|$ and $R_{nm}(\boldsymbol{r}) = |\boldsymbol{r}-\boldsymbol{r}_{m,n}|$, where $\boldsymbol{r}_{m,n}$ denotes the location of the (m,n) meta-atom. Equation 1 offers several important insights. First, we note that the leading term E_1^{SISO} represents the system response of continuous metasurface but corrected by a multiplicative factor of $B_1^{SISO} = \frac{2}{\pi} \sim 0.64$ (corresponding to about 3 dB energy loss). Meanwhile, the perturbation terms characterize the unwanted parasitic beams that divert the energy from the source into directions other than that of the intended receiver due to the one-bit quantization of the meta-atom programmability.

To illustrate the roles of different terms, we plot spatial maps of $\left|\widehat{\mathcal{H}}_{SISO}\right|$ for representative cases. Firstly, we consider two cases for which the source and intended receiver are in the near field of the meta-surface. For a receiver on or off the 0° azimuth, Fig. 2a and 2b respectively show plots of $\left|\widehat{\mathcal{H}}_{SISO}\right|$ both with continuous and one-bit coding metasurfaces. Additionally, the first a few nonzero terms $\left|E_p^{SISO}\right|$ are visualized. In both cases, we observe that the leading term $p=1$ dominates the system response $\left|\widehat{\mathcal{H}}_{SISO}\right|$ and there is no significant difference between the continuous coding and one-bit coding. While the focus is about 3 dB weaker with the one-bit coding, and the quantization energy loss is statistically uniformly distributed over the entire space. Overall, in these two cases the performance of one-bit coding is of comparable quality to that with the continuous coding.

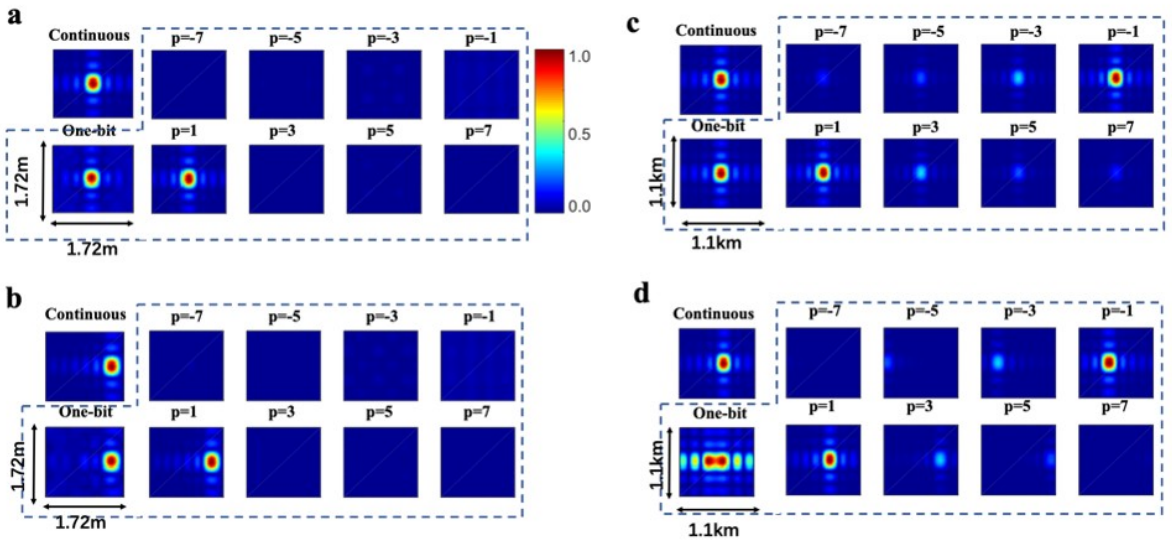

Figure 2 Spatial maps of $\left|\widehat{\mathcal{H}}_{\mathrm{SISO}}\right|$ for continuous and one-bit coding metasurfaces, as well as the maps of $\left|E_p^{\mathrm{SISO}}\right|$ for $p = \pm1, \pm3, \pm5, \pm7$ in the one-bit coding case, in which the maps titled with continuous are normalized their own maximums, and other maps are normalized by $\left|E_1^{SISO}\left(\boldsymbol{r}', \boldsymbol{r}';\right)\right|$. Different source and receiver locations are considered: a) $\boldsymbol{r}_s = (0, 0, 1.2\ \mathrm{m}), \boldsymbol{r}_q = (0, 0, 3\ \mathrm{m})$. b) $\boldsymbol{r}_s = (0, 0, 1.2\ \mathrm{m}), \boldsymbol{r}_q = (0, 0.6\ \mathrm{m}, 3\ \mathrm{m})$. c) $\boldsymbol{r}_s = (0, 0, 1\ \mathrm{km}), \boldsymbol{r}_q = (0, 0, 2\ \mathrm{km})$. d) $\boldsymbol{r}_s = (0, 0, 1.2\ \mathrm{km}), \boldsymbol{r}_q = (0, 0.1\ \mathrm{km}, 2\ \mathrm{km})$.

Next, we consider two similar scenarios in Fig. 2c and 2d for which both source and intended receiver are in the far field region. Here, the perturbation terms ($p \neq 1$) have non-negligible contributions to the system responses $\left|\widehat{\mathcal{H}}_{SISO}\right|$ but can be truncated at the number of calculated terms $P = 3$ (RMSE $< 0.5\%$). Unless the receiver is at the 0° azimuth, multiple unwanted parasitic beams appear that interfere with the desired beam. In particular, the $p = -1$ term appears to be mirror-symmetrical with respect to the normal direction $\widehat{\boldsymbol{n}}$ of the one-bit coding metasurface. More details can be found in Appendix B.

To shed more light on these far-field limitations, we simplify the E_p^{SISO} terms under a farfield approximation:

$$E_p^{SISO}\left(\boldsymbol{r}, \boldsymbol{r}_s; q, s\right) \approx B_p^{SISO} MN \frac{\exp\left[jk\left(pr_q - r + (p-1)r_s\right)\right]}{rr_s} \exp\left(jp\phi_q\right), \text{ for } \hat{\boldsymbol{r}} - p\hat{\boldsymbol{r}}_q + (1-p)\hat{\boldsymbol{r}}_s \| \widehat{\boldsymbol{n}} \quad (2)$$

Here, we denote by the symbol $\boldsymbol{a}\|\boldsymbol{b}$ that the vector $\boldsymbol{a}$ is parallel to the vector $\boldsymbol{b}$.

Then the desired beam ($p = 1$) in the far-field approximation is

$$E_1^{SISO}\left(\boldsymbol{r}, \boldsymbol{r}_s; q, s\right) \approx B_1^{SISO} MN \frac{\exp\left[jk\left(r_q - r\right)\right]}{rr_s} \exp\left(j\phi_q\right), \quad \text{for } \hat{\boldsymbol{r}} = \hat{\boldsymbol{r}}_q \quad (3)$$

and there are multiple significant unwanted parasitic beams corresponding to the values of $p \neq 1$. In particular, the expression for the $p = -1$ term in the far-field region is written as

$$E_{-1}^{SISO}\left(\boldsymbol{r}, \boldsymbol{r}_s; q, s\right) \approx B_{-1}^{SISO} MN \frac{\exp\left[-jk\left(r_q + r - 2r_s\right)\right]}{rr_s} \exp\left(-j\phi_q\right), \text{ for } \hat{\boldsymbol{r}}_q + \hat{\boldsymbol{r}} + 2\hat{\boldsymbol{r}}_s \| \widehat{\boldsymbol{n}} \quad (4)$$

Here, $\left|B_1^{\mathrm{SISO}}\right| = \left|B_{-1}^{\mathrm{SISO}}\right|$ confirms the previous observation in Fig. 2d of mirror-symmetry to the desired beam in terms of amplitude; and now it is 180° out of phase with the desired beam.

For the special case with $\hat{\boldsymbol{r}}_q = \hat{\boldsymbol{r}}_s = \widehat{\boldsymbol{n}}$ from Fig. 2c, the focusing ability of the one-bit coding programmable metasurface is acceptable because all undesired beams (especially $p = -1$) point to the 0° azimuth direction. This assumption holds in this realistic scenario that the metasurface is normally illuminated by a plane wave, and the receiver is mounted at the 0° azimuth. However, focusing is only the prerequisite and not sufficient condition for our goal to use the programmable metasurface as information encoding. For concreteness, we consider phase shift keying (PSK).

When $\hat{\boldsymbol{r}}_q = \hat{\boldsymbol{r}}_s = \widehat{\boldsymbol{n}}$, we have

$$E_p^{SISO}\left(\boldsymbol{r}, \boldsymbol{r}_s; q, s\right) = B_p^{SISO} MN \frac{1}{rr_s} \exp\left(jp\phi_q\right) \quad (5)$$

Thus the SISO system response reads

$$\widehat{\mathcal{H}}_{\mathrm{SISO}}\left(\boldsymbol{r}_q, \boldsymbol{r}_s; q, s\right) = \frac{2MN}{rr_s} \sum_{p=1}^{\infty} B_p^{SISO} \cos\left(p\phi_q\right) \tag{6}$$

We observe that $\widehat{\mathcal{H}}_{\mathrm{SISO}}\left(\boldsymbol{r}_q, \boldsymbol{r}_s; q, s\right)$ is a real number in this case, preventing the metasurface from achieving high-level PSK beyond BPSK.

2.2 Case II. SIMO and MIMO

We first consider the SIMO setting, in which a single source at $\boldsymbol{r}_s$ is linked to $Q(Q > 1)$ receivers via directive radiation beams, upon interacting with the metasurface. The q th beam is aimed at the intended receiver at $\boldsymbol{r}_q$ with desired phase $\phi_q\,(0 \leqslant \phi_q < 2\pi)$ for the PSK information encoding. For this purpose, the closed-loop estimate of the required one-bit control coding pattern of the metasurface is $\mathcal{C}_{m,n}^{SIMO} = \mathrm{sign}\left[\sum_{q=1}^{Q} \cos\left(\tilde{\phi}_{nm}^{SIMO}(q)\right)\right]$, where $\tilde{\phi}_{nm}^{SIMO}(q) \equiv \tilde{\phi}_{m,n}\left(\boldsymbol{r}_q; \boldsymbol{r}'\right)$.Following similar steps as before, we obtain the system response of the one-bit coding metasurface at $\boldsymbol{r}$ as:

$$\widehat{\mathcal{H}}_{SIMO}\left(\boldsymbol{r}, \boldsymbol{r}'; \{q\}, s\right) = \underbrace{E_1^{SIMO}\left(\boldsymbol{r}, \boldsymbol{r}'; \{q\}, s\right)}_{\text{leading term}} + \underbrace{\sum_{\{p_q\}/\left\{\sum_q |p_q|=1 \& p_q \neq -1\right\}} E_{\{p_q\}}^{SIMO}\left(\boldsymbol{r}, \boldsymbol{r}'; \{q\}, s\right) \exp\left[j \sum_{q=1}^{Q} p_q \phi_q\right]}_{\text{perturbation terms}} \tag{7}$$

Here, $\{q\}$ denotes a collection of Q receivers at different locations, and $\{p_q\}$ is a collection of Q harmonic orders which comes from the aforementioned Q receivers one by one. In Eq. 7,

$$E_1^{SIMO}\left(\boldsymbol{r}, \boldsymbol{r}'; \{q\}, s\right) = B_1^{SIMO} \sum_{q=1}^{Q} \exp\left(j\phi_q\right) A_1^{SISO}\left(\boldsymbol{r}, \boldsymbol{r}'; q, s\right)$$

$$E_{\{p_q\}}^{SIMO}\left(\boldsymbol{r}, \boldsymbol{r}'; \{q\}, s\right) = B_{\{p_q\}}^{SIMO} A_{\{p_q\}}^{SIMO}\left(\boldsymbol{r}, \boldsymbol{r}'; \{q\}, s\right)$$

where $B_{\{p_q\}}^{SIMO} = -\frac{j}{\pi} j^Q \sum_{q=1}^{Q} p_q \int_{-\infty}^{\infty} \frac{1}{\xi} \prod_{q=1}^{Q} J_{p_q}(\xi) d\xi$, $B_0^{SIMO} = \frac{1}{\pi} \int_{-\infty}^{\infty} \frac{1}{\xi} J_1(\xi) J_0^{Q-1}(\xi) d\xi$ and $A_{\{p_q\}}^{SIMO}\left(\boldsymbol{r}, \boldsymbol{r}'; \{q\}, s\right) = \sum_{m,n} \frac{\exp\left(j\left[\sum_{q=1}^{Q} p_q \Delta_{m,n}(\boldsymbol{r}_q; \boldsymbol{r}_s) - \Delta_{m,n}(r; \boldsymbol{r}')\right]\right)}{R_{nm}(\boldsymbol{r}) R_{nm}(\boldsymbol{r}')}$ .Note that $B_{\{p_q\}}^{SIMO} = 0$ when $\sum_{q=1}^{Q} |p_q|$ is an even number. More details about Eq. 7 are presented in Appendix C. As before, the Q-fold multiple summation of the second term in Eq. 7 can be approximated with an accuracy of RMSE $< 0.5\%$ under the condition of $\sum_q |p_q| \leqslant 3$.

Similar to the case of SISO, the leading term E_1^{SIMO} in Eq. 7 describes the system response of the corresponding continuous metasurface but with a multiplicative factor of B_1^{SIMO}. The collection $\{p_q\} / \left\{\sum_q |p_q| = 1 \& p_q \neq -1\right\}$ describe the energy leakages due to the one-bit quantization in comparison to the continuous coding metasurface. Moreover, signal interferences and cross talks between different intended receivers arise due to the one-bit coding, which will be studied in the subsequent section. For completeness, a generalization of the presented SIMO results to the MIMO situation has been included in Appendix D.

Before closing this section, we provide more insights into the relation of the system response between the one-bit and continuous coding metasurface. To that end, we accurately construct the system response of the continuous metasurface by linearly weighting K system responses of the one-bit coding metasurface. Note that these K system responses correspond to K different coding patterns of the one-bit coding metasurface. The K coding patterns of the one-bit metasurface can be designed such that the one-bit coding metasurface will produce the same radiation patterns but with K distinct radiation phases (i.e., K-level PSK) at the locations of the intended receivers. We illustrate it in the following for the SISO case. Assuming that the desirable system response of a continuous coding metasurface has the phase $\phi(0 \leqslant \phi < 2\pi)$ at an intended receiver at $\boldsymbol{r}$, then the desirable system response of the continuous coding metasurface can be constructed. With reference to Eq. 1, the one-bit coding metasurface with the k

th coding pattern will produce the system response $\widehat{\mathcal{H}}_{\mathrm{SISO}}^{(k)}(\mathbf{r};q,s)$ with the intended phase $\phi_q^{(k)}$ at the receiver at $\boldsymbol{r}_q(k=1,2,\ldots,K)$. Then, substituting Eq.1 into the first term $A_1^{SISO}(\boldsymbol{r},\boldsymbol{r}';q,s)$ in Eq. A3 leads to the following $2P$ linear equations:

$$\begin{cases} \sum_{k=1}^{K} w_k \exp\left(j\phi_q^{(k)}\right) = \frac{\pi}{2}\exp(j\phi) + \epsilon \\ \sum_{k=1}^{K} w_k \exp\left(jp\phi_q^{(k)}\right) = \epsilon, \quad p=-1,\pm 2,\ldots,\pm P \end{cases} \tag{8}$$

Herein, ϵ denotes the approximation error. To determine the K weighting factors $\{w_k\}$, a classical minimum mean-least-square method can be applied to Eq. 8. We find that when the receiver and/or sources are not in the "blind district" of the one-bit coding metasurface (i.e. the perturbation terms are negligible compared to the leading term), we can use the one-bit coding metasurface with 2 different control coding patterns to approximate the system response of the ideal metasurface. A thorough study of the minimum required value of K in the SIMO case is provided in Discussion 5 of Appendix C. Interestingly, we observe a clear link between the required minimum value of K to approximate the ideal metasurface response reasonably well and the ratio $Q/\gamma_{one-bit}$, where $\gamma_{one-bit}$ is the multiplicative factor $\left(B_1^{SISO}, B_1^{\mathrm{SIMO}} \text{ or } B_1^{MIMO}\right)$ between the desired $p=1$ one-bit coding system response term with and the continuous coding system response. (See details in Appendix C).

3 Signal interferences due to one-bit coding

The one-bit quantization of the coding metasurface gives rise to the quantization-related signal interferences between different channels in SIMO and MIMO settings. In the context of wireless communication, this yields so-called channel cross talk; while in the context of sensing, this results in image blurring. We now study this effect for concreteness in SIMO, but the developed results can easily be extended to MIMO. Throughout this section, we assume that the source and receivers are not in the "blind district", i.e., the perturbation terms are negligible compared to the leading term. We consider an information stream with M_i-level PSK modulation, where the source emits waves and the PSK information modulation is accomplished upon interaction with the metasurface, and the waves are directed to the desired receivers. We stress that it is not the source but the metasurface that performs the PSK modulation. The list of possible desired phases at the i th receiver (located at $\boldsymbol{r}_i$) is

$$\phi_i \in \theta_i + \left\{0, \frac{2\pi}{M_i}, 2\frac{2\pi}{M_i}, \ldots, (M_i-1)\frac{2\pi}{M_i}\right\}, \quad i=1,2,\ldots,Q$$

where the symbol θ_i denotes the phase bias for the i th receiver.

We here consider a realistic scenario, where any two receivers are well separated in terms of the Rayleigh limit, $\left|A_1^{SISO}(\boldsymbol{r}_i,\boldsymbol{r}_s;q,s)\right| \approx 0$ for $i \neq q$. Then, as detailed in Appendix E, we can obtain the coherence of $\widehat{\mathcal{H}}_{SIMO}(\boldsymbol{r}_i,\boldsymbol{r}_s;\{q\},s)$ and $\widehat{\mathcal{H}}_{SIMO}(\boldsymbol{r}_j,\boldsymbol{r}_s;\{q\},s)$:

$$\begin{aligned} &\left\langle \widehat{\mathcal{H}}_{SIMO}(\boldsymbol{r}_i,\boldsymbol{r}_s;\{q\},s), \widehat{\mathcal{H}}_{SIMO}(\boldsymbol{r}_j,\boldsymbol{r}_s;\{q\},s) \right\rangle = \\ &\qquad B_0^{SIMO} A_0 \sum_{n_{p:1\to Q/n_i}} Z^*_{\{M_p n_p \theta_p\}} E^{SIMO,*}_{\{M_p n_p\}}(\boldsymbol{r}_j;\{q\},s) \\ &\qquad + B_0^{SIMO,*} A_0^* \sum_{n_{p:1\to Q/n_j}} Z_{\{M_p n_p \theta_p\}} E^{SIMO}_{\{M_p n_p\}}(\boldsymbol{r}_i;\{q\},s), \quad \text{for } i \neq j. \end{aligned} \tag{9}$$

$$\left\langle \left|\widehat{\mathcal{H}}_{SIMO}(\boldsymbol{r}_i,\boldsymbol{r}_s;\{q\},s)\right|^2 \right\rangle \approx \left|B_0^{SIMO} A_0\right|^2$$

where $Z_{\{p_q\theta_q\}} = \exp\left(j\sum_q p_q\theta_q\right)$, and we have assumed that $A_0 \approx A_1^{SISO}(\boldsymbol{r}_i,\boldsymbol{r}_s;i,s)$ holds for any $\boldsymbol{r}_i \in \{q\}$ when the receivers are in a relative small range. Moreover, the superscript symbol $*$ denotes the complex conjugate operation. We can observe that the coherence function depends on the choice of the phase bias $\{\theta_i\}$, implying that the quantization-related signal interference can be improved by optimizing the setting of the phase bias $\{\theta_i\}$. This observation is consistent with the results presented at the end of this section in the context of holography.

To rigorously evaluate additional signal interference originating from the one-bit quantization of the metasurface, we now examine the statistical behavior of a given digital information symbol transferred through a given wireless SIMO channel while simultaneously the remaining SIMO links are deployed for other (statistically independent) digital information streams. For the digital information symbol acquired at $\boldsymbol{r}_u$, the statistical mean $\mu_u^{SIMO} = \left\langle \widehat{\mathcal{H}}_{SIMO}\left(\boldsymbol{r}_u, \boldsymbol{r}_s; \{q\}, s\right)\right\rangle$ and variance $\sigma_u^{SIMO} = \left\langle \left| \widehat{\mathcal{H}}_{SIMO}\left(\boldsymbol{r}_u, \boldsymbol{r}_s; \{q\}, s\right) - \left\langle \widehat{\mathcal{H}}_{SIMO}\left(\boldsymbol{r}_u, \boldsymbol{r}_s; \{q\}, s\right)\right\rangle \right|^2 \right\rangle$ are readily derived as:

$$\mu_u^{SIMO} = B_0^{SIMO} \underbrace{A_1^{SISO}\left(\boldsymbol{r}_u, \boldsymbol{r}_s; u, s\right) \exp\left(j\phi_u\right)}_{\text{for continuous coding metasurface}} + \underbrace{\sum_{\{p_q\}/\{\Sigma_q |p_q|=1 \& p_q \neq -1\}} E_{\{p_q\}}^{SIMO}\left(\boldsymbol{r}_u, \boldsymbol{r}_s; \{q\}, s\right) \exp\left[j p_u \phi_u\right] Z_{\{p_q\theta_q\}/p_u\theta_u} \prod_{q=1, q\neq u}^{Q} \delta_{p_q - n_q M_q}}_{\text{one-bit quantization mean bias}} \tag{10a}$$

$$\sigma_u^{SIMO} = \left|B_0^{SIMO}\right|^2 \underbrace{\sum_{q=1, q\neq u}^{Q} \sigma_q^2 \left\lfloor A_1^{SISO}\left(\boldsymbol{r}_u, \boldsymbol{r}_s; q, s\right)\right\rfloor^2}_{\text{for continuous coding metasurface}} + \underbrace{\chi\left(u, \{M_q\}\right)}_{\text{one-bit quantization variance}} \tag{10b}$$

Herein, $Z_{\{p_q\theta_q\}/p_u\theta_u} = \exp\left(j\sum_{q,q\neq u} p_q\theta_q\right)$, σ_q^2 is the covariance of the intended information stream of the q th receiver. In addition, the factor $\chi\left(u, \{M_q\}\right)$ characterizes the signal interferences arising from the one-bit quantization of the coding metasurface, see Appendix F. Furthermore, for the whole SIMO system, the variance can be approximated by taking average of $\left\{\sigma_u^{SIMO}\right\}$ over all intended receivers. As a result, we have:

$$\begin{aligned} \sigma_{\text{SIMO}}^2 &= \frac{1}{Q}\sum_{u=1}^{Q} \sigma_u^{SIMO} \\ &= \left|B_0^{SIMO}\right|^2 \underbrace{\frac{1}{Q}\sum_{u=1}^{Q}\sum_{q=1, q\neq u}^{Q} \sigma_q^2 \left\lfloor A_1^{SISO}\left(\boldsymbol{r}_u, \boldsymbol{r}_s; q, s\right)\right\rfloor^2}_{\sigma_{\text{cont}}^2} + \underbrace{\frac{1}{Q}\sum_{u=1}^{Q}\chi\left(u, \{M_q\}\right)}_{\chi} \end{aligned} \tag{11}$$

If an continuous coding metasurface is used instead, variance and mean are characterized by σ_{cont}^2 and $A_1^{SISO}\left(\boldsymbol{r}_u; u, s\right)\exp\left(j\phi_u\right)$ Therefore, the effect of the one-bit quantization of the metasurface is obvious from Eq. 10: the one-bit quantization induced mean bias as well as the additional noise due to the one-bit quantization variance both reduce the distinguishability of distinct information symbols.

4 Difference in information capacity of one-bit vs ideal metasurface

In this section, based on the above-established results, we investigate the relation between the information capacities of a metasurface with one-bit coding and a metasurface with continuous coding. Based on Shannon's theory, the information capacity $\mathcal{C}_{\text{cont}}$ of an continuous coding metasurface can be readily obtained [54, 55]. For instance, for the SIMO case, it reads $\mathcal{C}_{\text{cont}} = Q\log_2\left(1 + S/\left(\sigma_n^2 + \sigma_{\text{cont}}^2\right)\right)$ per frequency, where S and σ_n^2 denote the signal and system noise levels, respectively, and $S = \mathcal{P}\left|A_1^{\text{SISO}}\left(\boldsymbol{r}_q, \boldsymbol{r}_s; q, s\right)\right|^2 \approx \mathcal{P}\left|MN/r_s r_q\right|^2$ (far-field approximation). The one-bit quantization of the metasurface has two consequences: (i) an energy loss by a factor of $\gamma_{one-bit}^2$, and (ii) additional noise $\sigma_{\text{one-bit}}^2$. Both effects deteriorate the SNR (signal-to-noise ratio) and thereby reduce the information capacity in the case of the one-bit coding metasurface:

$$\mathcal{C}_{\text{one-bit}} \approx Q\log_2\left(1 + \gamma_{\text{one-bit}}^2\, S/\left(\sigma_n^2 + \sigma_{\text{one-bit}}^2\right)\right) \tag{12}$$

where $\gamma_{one-bit} = \begin{cases} B_1^{\text{SISO}}, & \text{for SISO} \\ B_1^{\text{SIMO}}, & \text{for SIMO} \\ B_1^{\text{MIMO}}, & \text{for MIMO} \end{cases}$ and $\sigma^2_{\text{one-bit}} = \begin{cases} 0, & \text{for SISO} \\ \sigma^2_{SIMO}, & \text{for SIMO} \\ \sigma^2_{\text{MIMO}}, & \text{for MIMO} \end{cases}$

The approximate-equal symbol in Eq. 12 is used because the one-bit quantization mean bias in Eq. 11 decreases the distinguishable distance between two different information symbols, which will decrease the achievable information capacity. Now, taking the SIMO as an illustrative example, we can derive the relation between $\mathcal{C}_{\text{cont}}$ and $\mathcal{C}_{\text{one-bit}}$ as

$$\frac{\Delta\mathcal{C}}{Q} = \frac{C_{\text{one-bit}} - C_{\text{cont}}}{Q} \approx \log_2\left(\gamma^2_{\text{one-bit}}\,\frac{\sigma_n^2+\sigma^2_{\text{cont}}}{\sigma_n^2+\sigma^2_{\text{one-bit}}}\right) \approx \log_2\left(\gamma^2_{\text{one-bit}}\,\frac{\sigma_n^2+\sigma^2_{\text{cont}}}{\sigma_n^2+\gamma^2_{\text{one-bit}}\,\sigma^2_{\text{cont}}+\chi}\right) \tag{13}$$

where we assumed $SNR \gg 1$and $\sigma^2_{\text{one-bit}} = \gamma^2_{\text{one-bit}}\,\sigma^2_{\text{cont}} + \chi$ in Eq. 13, respectively. Note that the definition in Eq. 13 implies $\Delta\mathcal{C} \leqslant 0$. Considering that $\frac{\Delta\mathcal{C}}{Q}$ behaviors as a monotone decreasing function of σ_n^2 for $\sigma^2_{\text{cont}} > \sigma^2_{\text{one-bit}}$, we can estimate its lower and upper bounds:

$$\log_2\left(\gamma^2_{\text{one-bit}}\right) \leqslant \frac{\Delta\mathcal{C}}{Q} \leqslant \log_2\left(\frac{\gamma^2_{\text{one-bit}}\,\sigma^2_{\text{cont}}}{\gamma^2_{\text{one-bit}}\,\sigma^2_{\text{cont}}+\chi}\right) \tag{14}$$

The upper bound of $\frac{\Delta\mathcal{C}}{Q}$ is reached when the system noise level σ_n^2 is relatively low $\left(\sigma_n^2 \ll \sigma^2_{\text{cont}}\right.$ and $\left.\sigma_n^2 \ll \gamma^2_{\text{one-bit}}\,\sigma^2_{\text{cont}}+\chi\right)$. Furthermore, if $\chi \ll \gamma^2_{\text{one-bit}}\,\sigma^2_{\text{cont}}$, the upper bound approaches to zero, i.e., $\frac{\Delta C}{Q} \to 0$, which implies that the one-bit coding metasurface has nearly the same information capacity as the continuous metasurface under these conditions. We will see in Fig. 6 that the inequality $\chi \ll \gamma^2_{\text{one-bit}}\,\sigma^2_{\text{cont}}$ holds when the number of channels Q is small and lowlevel PSK is used. In this case, the adverse effect of lower signal intensity due to one-bit coding is counterbalanced by a lower signal interference.

5 Results and discussions

5.1 Information-encoding capabilities of one-bit coding metasurface

We consider the SISO case, and systematically study the information-encoding capabilities of the one-bit coding metasurface in wireless communications with M_q-level PSK, which can ideally achieve the phase quantization of $\widehat{\mathcal{H}}_{\text{SISO}}$ as: $\phi_q \in \left\{\frac{2\pi(i-1)}{M_q}, i = 1, 2, \ldots, M_q\right\}$. To quantify to what extent the one-bit coding metasurface is capable of approaching these desired values, we define the following metric for the achievable phase resolution:

$$\Delta\varphi_{\text{SISO}}\left(\boldsymbol{r}_q\right) = \min_{i,j}\left|\varphi^{(i)}_{\text{SISO}}\left(\boldsymbol{r}_q\right) - \varphi^{(j)}_{\text{SISO}}\left(\boldsymbol{r}_q\right)\right| \tag{15}$$

where $\varphi^{(i)}_{\text{SISO}}$ is the phase of $\widehat{\mathcal{H}}_{\text{SISO}}$ for the i th intended phase. To quantify the difference between the performance with one-bit and ideal coding, we define the following metric:

$$EC^{SISO} = \frac{1}{MN}\sum_{m,n}\left|\text{sign}\left[\cos\left(\tilde{\phi}^{\text{SISO}}_{nm}\right)\right] - \cos\left(\tilde{\phi}^{\text{SISO}}_{nm}\right)\right| \tag{16}$$

Figure 3a and Figure 3e plot the dependence of $\Delta\varphi_{SISO}\left(\boldsymbol{r}_q\right)$ and EC^{SISO}, respectively, on $\boldsymbol{r}_q$ for QPSK ($M_q = 4$) with a normally incident source deployed at a distance of 2 km from metasurface, i.e. in its far-field. The ability of the one-bit coding metasurface to perform QPSK information encoding with high fidelity is immediately obvious, except for the case when the receiver is on the azimuth 0° and in the far-field region. This result is in line with our above-mentioned interpretation of Eq. 6. In a scenario with a source incident at an oblique angle, as shown in Figure 3d and Figure 3f, there appears to be a similar limitation if $\hat{\boldsymbol{r}}_q + \hat{\boldsymbol{r}}_s \| \widehat{\boldsymbol{n}}$. Indeed, in this case the far-field approximation of $\tilde{\phi}^{\text{SISO}}_{nm}$ reads

$$\begin{aligned} \tilde{\phi}^{\text{SISO}}_{nm} &= k\left(\left|\boldsymbol{r}_s - \boldsymbol{r}_{m,n}\right| + \left|\boldsymbol{r}_q - \boldsymbol{r}_{m,n}\right|\right) + \phi_q \approx k\left(r_s + r_q - \boldsymbol{r}_{m,n}\cdot\left(\hat{\boldsymbol{r}}_s + \hat{\boldsymbol{r}}_q\right)\right) + \phi_q \\ &\approx k\left(r_s + r_q\right) + \phi_q \quad \text{for } \hat{\boldsymbol{r}}_q + \hat{\boldsymbol{r}}_s \| \hat{\boldsymbol{n}} \end{aligned} \tag{17}$$

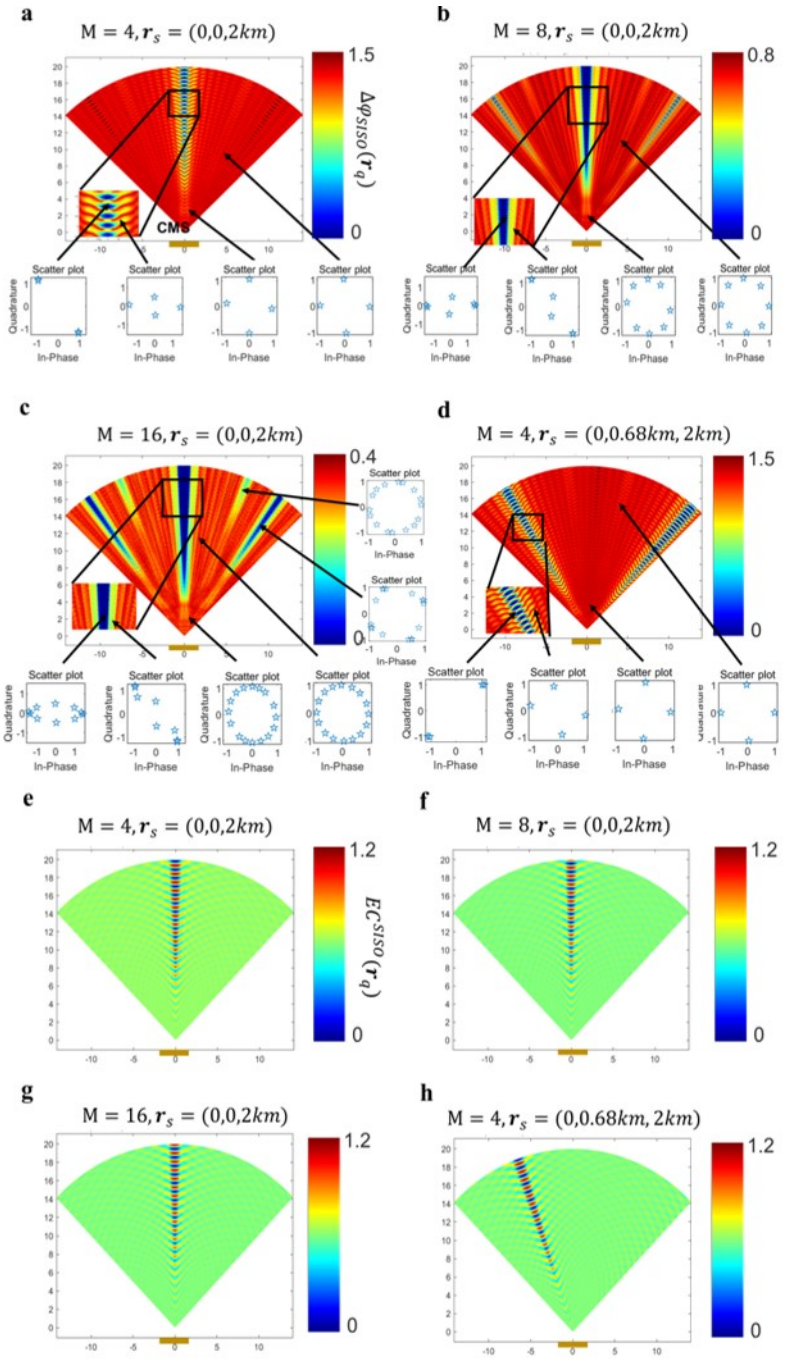

Figure 3 Fig. 3. M-level PSK with a one-bit coding programmable metasurface in SISO. a-d) Dependence of phase resolution $\Delta\varphi_{\mathrm{SISO}}$ on the receiver's location $\boldsymbol{r}_q$. Considered receiver locations are within a distance between 0 and 20 m from the metasurface for an azimuth between -45° and 45°. The insets provide representative constellation diagrams. Different levels of PSK and source location are considered, as indicated in the subfigure titles. e-h) Dependence of EC^{SISO} on $\boldsymbol{r}_q$ for the same settings as in a-d. In addition, the metasurface has been marked with a yellow solid rectangular.

such that the control coding pattern of the one-bit coding programmable metasurface is $\mathcal{C}_{m,n}^{\mathrm{SISO}} = \mathrm{sign}\left[\cos\left(k\left(r_s + r_q\right) + \phi_q\right)\right]$. Again, it is obvious why a receiver in the far field with $\hat{\boldsymbol{r}}_q + \hat{\boldsymbol{r}}_s \| \widehat{\boldsymbol{n}}$ cannot distinguish M_q-level PSK information if $M_q > 2$. In such cases, PSK must be limited to $M_q = 2$ (BPSK). The pronounced increase of EC^{SISO} for this scenario in Figure 3e,h further confirms that this limitation is attributed to the one-bit coding of the programmable metasurface.

Higher-order PSKs with $M_q = 8$ and $M_q = 16$ are considered in Figure 3b-c and Figure 3f-g in terms of $\Delta\varphi_{\mathrm{SISO}}\ (\boldsymbol{r}_q)$ and EC^{SISO}, respectively. In light of the well-known reciprocal property [56], we conclude that the one-bit coding metasurface is capable of efficiently manipulating the EM information at least up to 16-level PSK in the considered setup, if the source and receiver are deployed in the near-field region (see Appendix G). In general, efficient manipulation of EM information becomes increasingly challenging as M_q increases due to the increasing importance of unwanted parasitic beams.

Throughout our paper, we have assumed an 'ideal' one-bit quantization of the programmable metasurface. Specifically, we assumed that upon switching the meta-atom from its ' 0 ' (or ' 1 ') state to its ' 1 ' (or ' 0 ') state, the reflection phase experiences a change of 180° while the reflection amplitude remains unchanged. However, such ideal one-bit quantization cannot be realized in practice for many reasons, including non-ideal active lumped elements (e.g., the PIN diode) and fabrication errors. The reflection response of the non-ideal one-bit meta-atom is $A_+ e^{j\phi_+}$ and $A_- e^{j\phi_-}$ for states ' 1 ' and ' 0 ' (with $0 \leqslant A_\pm \leqslant 1$), respectively, instead of 1 and -1. The methodology developed in our paper can be readily generalized to non-ideal one-bit meta-atoms. Specifically, the radiation signal for the non-ideal one-bit quantization $\widehat{\mathcal{H}}_{SISO,SIMO,MIMO}^{\text{non-ideal}}(\mathbf{r};\ldots)$ is

$$\widehat{\mathcal{H}}_{\mathrm{SISO,SIMO,MIMO}}^{\mathrm{non}}\left(\mathbf{r};\cdots\right) = \gamma_0 A_0^{\mathrm{SISO}}\left(\boldsymbol{r}; q\cdots\right) + \gamma_1 \widehat{\mathcal{H}}_{\mathrm{SISO,SIMO}\ ,MIMO}(\mathbf{r};\cdots) \tag{18}$$

where $\gamma_0 = \frac{\left(A_+ e^{j\phi_+} + A_- e^{j\phi_-}\right)}{2}$ and $\gamma_1 = \frac{\left(A_+ e^{j\phi_+} - A_- e^{j\phi_-}\right)}{2}$. It can be observed from Eq. 18 shown that, in terms of manipulating the radiation beam, the non-ideality of a one-bit quantized metasurface results in additional energy leakage. More discussions about the non-ideal one-bit quantization of programmable coding metasurfaces can be found in Appendix I .

5.2 Signal interference of one-bit coding metasurface

To illustrate the results and conclusions on signal interference, we consider a concrete and promising SIMO application: metasurface-generated holograms [32]. Specifically, we examine the capability of the one-bit coding metasurface to realize the holographic image of English letter 'K'.

We assume that the desired phases over the profile of the letter 'K' are randomly distributed, as shown in Figure 4a. The normalized amplitude and phase of the achieved holographic image at a distance of 3 m away from the one-bit coding metasurface is shown in the top row of Figure 4c, and the corresponding control coding pattern of the one-bit coding metasurface is reported. For comparison, the corresponding results obtained by the GS algorithm with and without the phase constraint are shown in the middle and bottom rows of Figure 4c. In both cases we initialize the GS algorithm with $\mathcal{C}_{m,n}^{SIMO}$. The convergence behavior of the GS algorithm with and without the phase constraint is plotted in Figure 4b. Our results show that the proposed closed-form formula for obtaining the coding pattern of the one-bit coding metasurface, $\mathcal{C}_{m,n}^{SIMO}$, gives satisfactory results with comparable quality to that achieved by the iterative GS algorithm. In both cases, the quantization-induced signal interference among different channels notably limits the quality of the holographic image. If the constraints are relaxed by ignoring the desired phases, the one-bit coding metasurface yields a holographic image of acceptable quality. A further possibility is to simplify the phase constraint by targeting a constant value for the entire letter 'K'. The corresponding results in Figure 5 for different targeted phase values reveal a setting, in which the one-bit coding metasurface produces acceptable holographic images in terms of both phase and amplitude. Then, it can be verified that the phase $\{\phi_q\}$ could provide controllable parameters to minimize the signal interference, as pointed out previously with respect to the phase bias $\{\theta_i\}$.

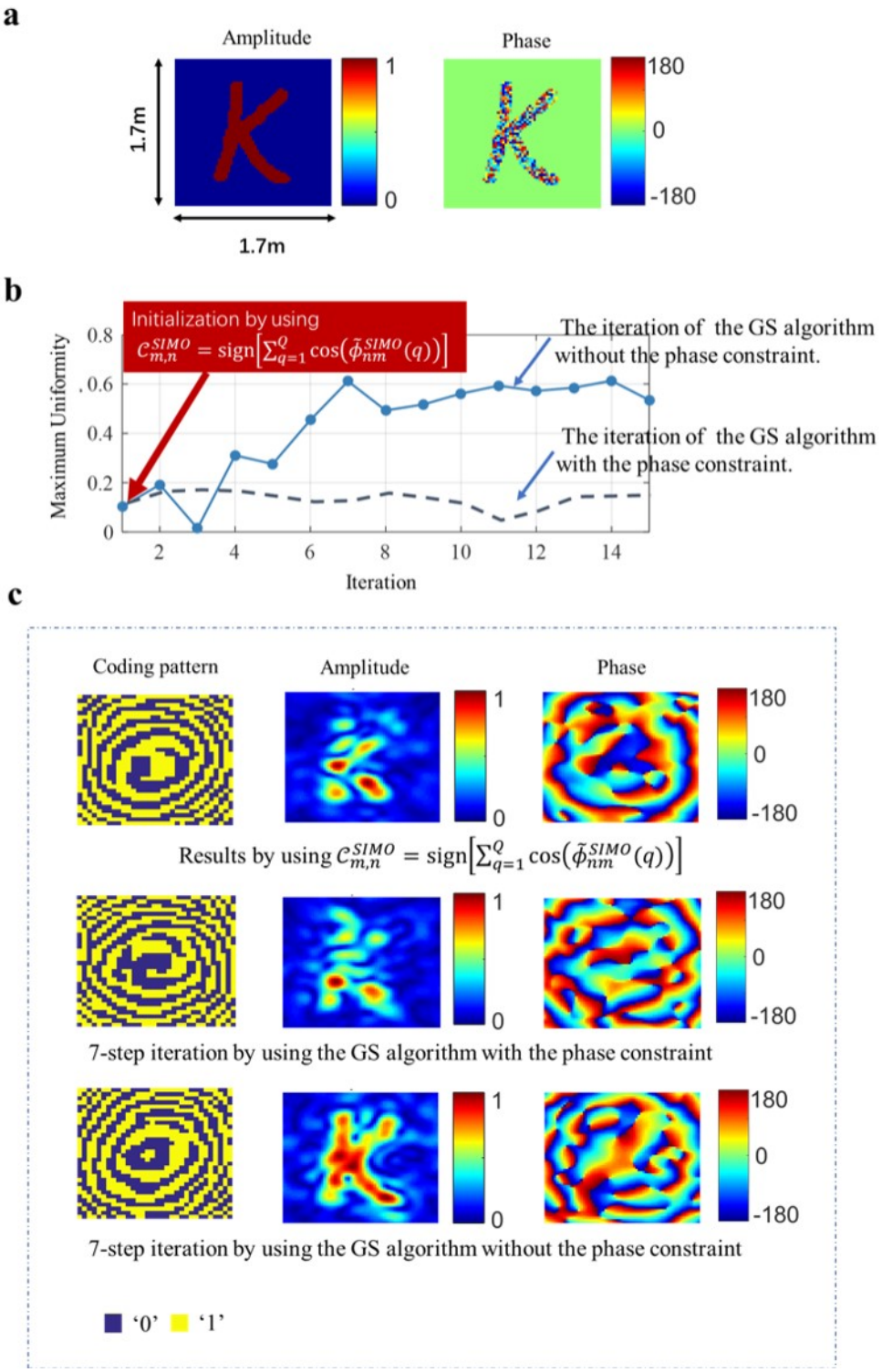

Figure 4 SIMO results for holographic imaging. The source is deployed at $(0, 0, 2$ m) and the observation plane is at a distance of 3 m from the one-bit coding metasurface. **a**. Amplitude (left) and phase (right) of the targeted hologram to be generated by the one-bit coding metasurface. b. Convergence of the GS algorithm with and without the phase constraint in terms of the maximum uniformity as figure of merit (see Eq. 1 in Ref. [53]). In both cases, the GS algorithm is initialized with $\mathcal{C}_{m,n}^{\mathrm{SIMO}} = \mathrm{sign}\left[\sum_{q=1}^{Q}\cos\left(\tilde{\phi}_{nm}^{\mathrm{SIMO}}(q)\right)\right]$. c. Results using $\mathcal{C}_{m,n}^{\mathrm{SIMO}}$ and Eq. 2 are shown in the top row, where the coding pattern of the one-bit metasurface, the amplitude and phase of the holographic image are shown on the left, middle and right, respectively. The corresponding results using the GS algorithm with and without the phase constraint are shown in the middle and bottom rows, respectively.

5.3 Information capability of one-bit and continuous coding metasurfaces

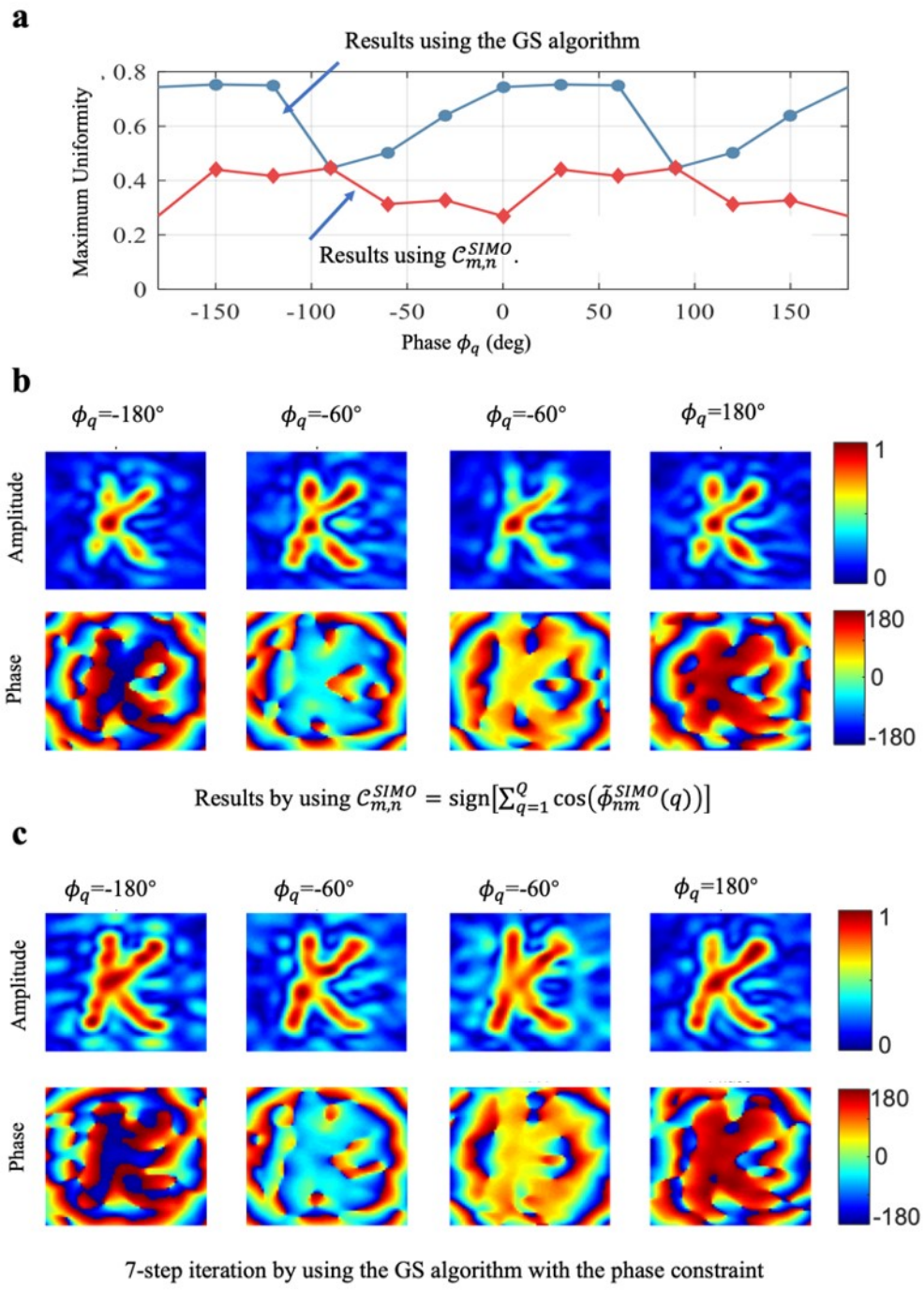

Figure 5 Relaxing phase constraints in the SIMO holography. The setup is the same as that in Figure 4 except that the phase of targeted holographic image is set to be constant rather than random. a. Image quality (evaluated in terms of the maximum uniformity) as a function of the targeted phase. b. Results with $\mathcal{C}_{m,n}^{\text{SIMO}}$ and Eq. 7 in terms of normalized amplitude and phase of the obtained holographic image. **c**. The corresponding results by the GS algorithm with the phase constraint.

We go on to evaluate the normalized difference in information capacities $\frac{\Delta\mathcal{C}}{Q}$ of the one-bit and continuous coding metasurfaces in the SIMO scenario. Figure 6a plots $\frac{\Delta\mathcal{C}}{Q}$ as a function of the number of channels Q for different system SNRs, and Figure 6b compares $\sigma_{one-bit}^2$ and σ_{cont}^2 as a function of the number of channels Q, in which the source and receivers are deployed in the near-field region of the metasurface. It

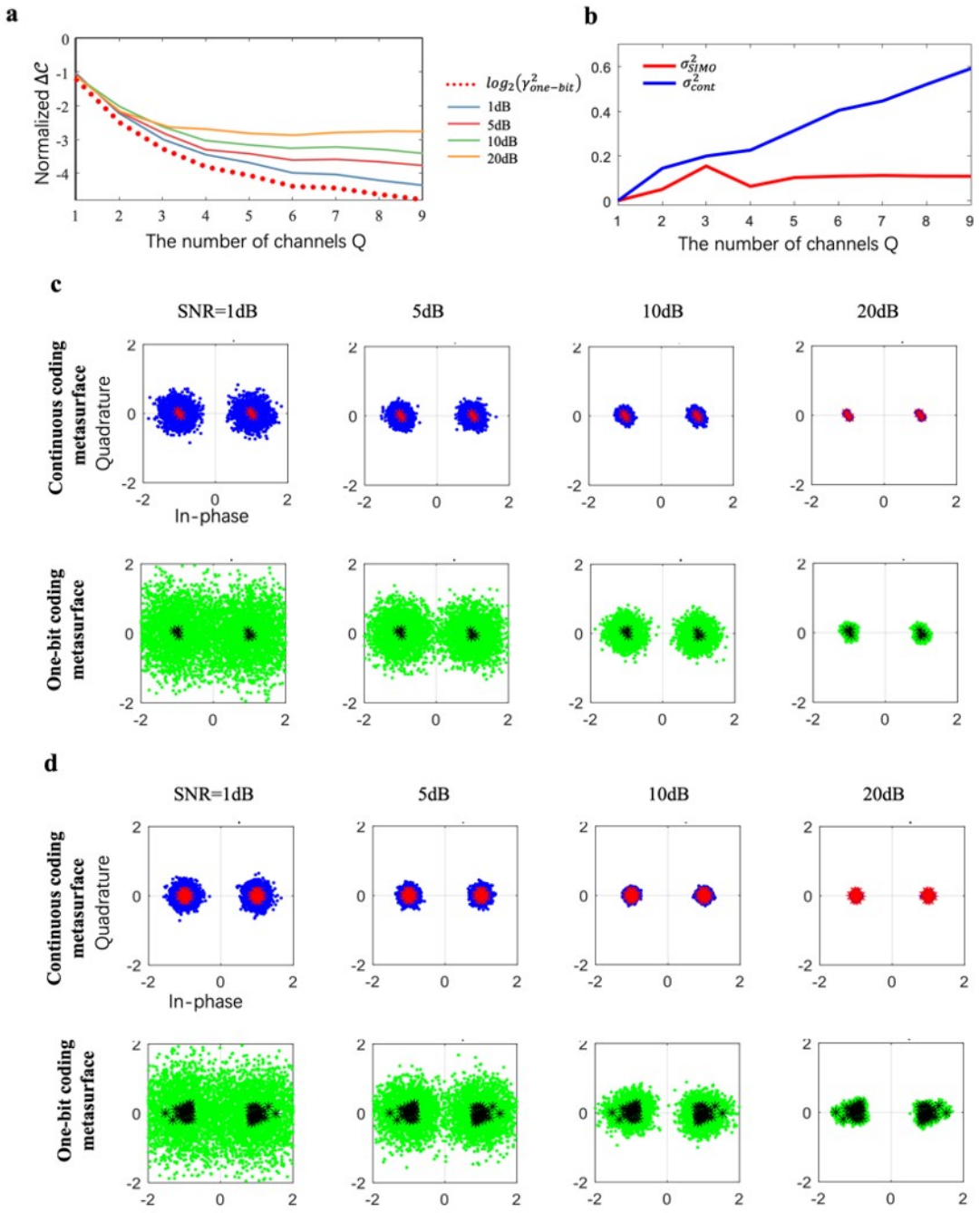

Figure 6 a. The normalized difference information capacity $\frac{\Delta c}{Q}$ in SIMO setting, in comparing the one-bit coding metasurface with the continuous metasurface in the SIMO scenario as a function of Q for different system SNRs when the receiver and source are in the near-field region of the metasurface. For comparison, the lower bound of $\frac{\Delta C}{Q}$ represented by $\log_2\left(\gamma^2_{\text{one-bit}}\right)$ is also plotted. The binary PSK ($M = 2$) is considered. b. The comparison of $\sigma^2_{\text{one-bit}}$ and σ^2_{cont} as a function of the number of channels Q. c, d. Constellation diagrams for $Q = 3$ and $Q = 6$ for different system SNRs. The constellation diagram axes are normalized by B_0^{SIMO}. Additionally, the red-marked and black-marked stars of the constellation diagrams characterize the signal interferences for the system-noise-free case, respectively. In this set of examinations, the source is located at $(0, 0, 1.2$ m), and the receivers are deployed at the distance of 3 m away from the metasurface.

can be verified from this set of figures that $\frac{\Delta \mathcal{C}}{Q}$ approaches to the upper bound identified in Eq. 16, and that the upper bound will tend to zero, as the system SNR is increased; in contrast, for low system SNRs the lower bound $\log_2\left(\gamma^2_{\text{one-bit}}\right)$ is approached. Some representative constellation diagrams for $Q = 3$ and $Q = 6$ for different system SNRs are shown in Figure 6c and d, in which the red and black stars characterize the signal interferences for the system-noise-free case, respectively. Additionally, the bit-

error analysis on the system of one-bit coding metasurface can be made along the same line, as detailed in Appendix H. It is obvious, in line with our previous calculations, that the one-bit quantization of the metasurface will give rise to additional signal interferences, and that such interferences will become stronger if the number of channels Q is larger. Nonetheless, it can be observed that the one-bit coding programmable metasurface performs almost as well as the continuous coding metasurface as long as Q is not too large.

6 Conclusions

We have explored fundamental limitations of the one-bit coding metasurfaces in comparison to the continuous coding metasurfaces in terms of their information capacity and considered illustrative examples from key applications in wireless communications and holography. Our results illustrate surprisingly nearly no performance deterioration due to the one-bit coding under mildly favorable constraints, such as low-level PSK, few-user SIMO or relaxed phase constraints on hologram. We expect that these fundamental insights will impact a wide range of metasurface-assisted techniques seeking to control the flow of information, both for electromagnetic waves and other frequencies and wave phenomena [45–52]. Looking forward, an avenue for the future research is to generalize the presented concepts to scattering rich environments [18,20,24] in which the scattering and reverberation will make the identification of suitable metasurface configurations more challenging; however, these seemingly adverse scattering effects can be leveraged as secondary sources that may further reduce the performance gap between the one-bit and continuous coding of the programmable metaatoms.

References

1 Foschini, G. J., Gans, M. J. On limits of wireless communications in a fading environment when using multiple antennas. Wirel. Pers. Commun., 1998, 6: 311
2 Goldsmith, A. Wireless Communications. ,Cambridge University Press, 2005.
3 Marzetta, T. L. Massive MIMO: An Introduction. Bell Labs Tech. J., 2015, 20, 11
4 Cho, Y. S., Kim, J., Yang, W. Y. Kang, C. MIMO-OFDM wireless communications with MATLAB. Wiley-IEEE Press, 2011
5 Cui, T. J., Qi, M. Q., Wan, X., Zhao, J. Cheng, Q. Coding metamaterials, digital metamaterials and programmable metamaterials. Light Sci. Appl., 2014,3, e218
6 Li, L. Cui, T. J. Information metamaterials – from effective media to real-time information processing systems. Nanophotonics, 2019, 8, 703
7 Wan, X. et al. Multichannel direct transmissions of near-field information. Light Sci. Appl., 2019, 8, 60
8 Zhao, J. et al. Programmable time-domain digital-coding metasurface for non-linear harmonic manipulation and new wireless communication systems. Natl. Sci. Rev., 2019, 6, 231–238
9 Cui, T. J., Liu, S., Bai, G. D. Ma, Q. Direct Transmission of Digital Message via Programmable Coding Metasurface. Research, 2019, 1–12
10 Shuang, Y., Zhao, H., Ji, W., Cui, T. J. Li, L. Programmable high-order OAM-carrying beams for direct-modulation wireless communications. IEEE J. Emerg. Sel. Top. Circuits Syst., 2020,10, 29
11 Ma, Q. et al. Smart metasurface with self-adaptively reprogrammable functions. Light Sci. Appl., 2019, 8, 98
12 Dai, L. et al. Reconfigurable intelligent surface-based wireless communications: antenna design, prototyping, and experimental Results. IEEE Access, 2020, 8, 45913
13 Renzo, M. D. et al. Smart radio environments empowered by reconfigurable AI meta-surfaces: an idea whose time has come. EURASIP J. Wirel. Commun. Netw., 2019, 129
14 Hu, S., Rusek, F. Edfors, O. Beyond Massive MIMO: The potential of data transmission with large intelligent surfaces. IEEE Trans. Signal Process., 2018, 66, 2746
15 Tang, W., Wong, K.-K., Li, X., Zhao, X. Jin, S. MIMO transmission through reconfigurable intelligent surface: system design, analysis, and implementation. IEEE J. Sel. AREAS. Commun., 2020,38, 17
16 Tang, W., Han, Y., Renzo, M. D., Zeng, Y. Jin, S. Wireless communications with reconfigurable intelligent surface: path loss modeling and experimental measurement. IEEE Trans. Wirel. Commun., 2021, 20, 19
17 Arun, V. Balakrishnan, H. RFocus: Beamforming using thousands of passive antennas. 17th USENIX Symposium on Networked Systems Design and Implementation (NSDI), 2020,1047
18 del Hougne, P., Fink, M. Lerosey, G. Optimally diverse communication channels in disordered environments with tuned randomness. Nat. Electron., 2019, 2, 36
19 Zhao, H. et al. Metasurface-assisted massive backscatter wireless communication with commodity Wi-Fi signals. Nat. Commun., 2020, 11, 3926
20 Imani, M. F., Smith, D. R. del Hougne, P. Perfect absorption in a disordered medium with programmable meta-atom inclusions. Adv. Funct. Mater., 2020, 30, 2005310
21 Sleasman, T., F. Imani, M., Gollub, J. N. Smith, D. R. Dynamic metamaterial aperture for microwave imaging. Appl. Phys. Lett., 2015, 107, 204104
22 Sleasman, T., Imani, M. F., Gollub, J. N. Smith, D. R. Microwave imaging using a disordered cavity with a dynamically tunable impedance surface. Phys. Rev. Appl., 2016,6, 054019
23 Li, Y. B. et al. Transmission-type 2-Bit programmable metasurface for single-sensor and single-frequency microwave imaging. Sci. Rep., 2016, 6, 23731
24 del Hougne, P., Imani, M. F., Fink, M., Smith, D. R. Lerosey, G. Precise localization of multiple noncooperative objects in a disordered cavity by wave front shaping. Phys. Rev. Lett., 2018, 121, 063901
25 Li, L. et al. Machine-learning reprogrammable metasurface imager. Nat. Commun., 2019 10, 1082

26 del Hougne, P., Imani, M. F., Diebold, A. V., Horstmeyer, R. Smith, D. R. Learned integrated sensing pipeline: reconfigurable metasurface transceivers as trainable physical layer in an artificial neural network. Adv. Sci.,2019,1901913
27 Li, H.-Y. et al. Intelligent electromagnetic sensing with learnable data acquisition and processing. Patterns , 2020,1, 100006
28 Li, L. et al. Intelligent metasurface imager and recognizer. Light Sci. Appl., 2019, 8, 97
29 Sleasman, T. et al. Implementation and characterization of a two-dimensional printed circuit dynamic metasurface aperture for computational microwave imaging. IEEE Trans. Antennas Propag., 2020, 1
30 Smith, D. R. et al. An analysis of beamed wireless power transfer in the Fresnel zone using a dynamic metasurface aperture. J. Appl. Phys., 2017, 121, 014901
31 del Hougne, P., Fink, M. Lerosey, G. Shaping microwave fields using nonlinear unsolicited feedback: application to enhance energy harvesting. Phys. Rev. Appl. , 2017,8, 061001
32 Li, L. et al. Electromagnetic reprogrammable coding-metasurface holograms. Nat. Commun., 2017, 8, 197
33 del Hougne, P. Lerosey, G. Leveraging chaos foir wave-based analog computation: demonstration with indoor wireless communication Signals. Phys. Rev. X, 2018, 8, 041037
34 Cui, T.-J., Liu, S. Li, L.-L. Information entropy of coding metasurface. Light Sci. Appl., 2016, 5, e16172
35 Wu, H. et al. Information theory of metasurfaces. Natl. Sci. Rev., 2020, 7, 561
36 Carcolé, E., Campos, J. Bosch, S. Diffraction theory of Fresnel lenses encoded in low-resolution devices. Appl. Opt., 1994, 33, 162
37 Carcolé, E., Campos, J. Juvells, I. Phase quantization effects on Fresnel lenses encoded in low resolution devices. Opt. Commun., 1996, 132, 35
38 Alais, P. Fink, M. Fresnel zone focusing of linear arrays applied to B and C echography. Acoustical Holography,1977,Springer US
39 Derode, A., Tourin, A. Fink, M. Ultrasonic pulse compression with one-bit time reversal through multiple scattering. J. Appl. Phys., 2014, 85, 6434
40 Turtaev, S. et al. Comparison of nematic liquid-crystal and DMD based spatial light modulation in complex photonics. Opt. Express, 2017, 25, 29874
41 Badiu, M.-A. Coon, J. P. Communication through a large reflecting surface with phase errors. IEEE Wirel. Commun. Lett., 2020, 9, 184
42 Zhang, H., Di, B., Song, L. Han, Z. Reconfigurable intelligent surfaces assisted communications with limited phase shifts: how many phase shifts are enough? IEEE Trans. Veh. Technol., 2020, 69, 4498
43 Li, D. Ergodic capacity of intelligent reflecting surface-assisted communication systems with phase errors. IEEE Commun. Lett., 2020, 24, 1646
44 Xu, P., Chen, G., Yang, Z. Di Renzo, M. Reconfigurable intelligent surfaces assisted communications with discrete phase shifts: how many quantization levels are required to achieve full diversity? IEEE Wirel. Commun. Lett., 2020,1
45 Ou, J.-Y., Plum, E., Zhang, J. Zheludev, N. I. An electromechanically reconfigurable plasmonic metamaterial operating in the near-infrared. Nat. Nanotechnol., 2013, 8, 252
46 Arbabi, E. et al. MEMS-tunable dielectric metasurface lens. Nat. Commun. ,2018,9, 812
47 Chen, H.-T. et al. Active terahertz metamaterial devices. Nature, 2006, 444, 597–600
48 Cong, L., Pitchappa, P., Lee, C. Singh, R. Active phase transition via loss engineering in a terahertz MEMS metamaterial. Adv. Mater., 2017, 29, 1700733
49 Wang, L. et al. A Review of THz modulators with dynamic tunable metasurfaces. Nanomaterials, 2019, 9, 965
50 Wang, Q. et al. Optically reconfigurable metasurfaces and photonic devices based on phase change materials. Nat. Photonics, 2016, 10, 60
51 Rout, S. Sonkusale, S. Wireless multi-level terahertz amplitude modulator using active metamaterial-based spatial light modulation. Opt. Express, 2016, 24, 14618
52 Watts, C. M. et al. Terahertz compressive imaging with metamaterial spatial light modulators. Nat. Photonics, 2014,8,605
53 Goerner, F. L., Duong, T., Stafford, R. J. Clarke, G. D. A comparison of five standard methods for evaluating image intensity uniformity in partially parallel imaging MRI: Measuring uniformity in MRI with partially parallel imaging. Med. Phys., 2013, 40, 082302
54 Shannon, C. E. A mathematical theory of communication. Bell Syst. Tech. J., 1948, 27, 379
55 Francis, T. Entropy and information optics: connecting information and time. CRC Press, 2017
56 Kong J. A. Electromagnetic wave theory. J Wiley Son, 1986

SCIENCE CHINA
Information Sciences

• Supplementary File •

One-bit quantization is good for programmable coding metasurfaces

Ya SHUANG †[1], Hanting ZHAO †[1], Menglin WEI[1], Qiang CHENG[2,3,4], Shi JIN[2,3,4], Tie Jun CUI[2,3,4], Philipp HOUGNE[5] & Lianlin LI[6]

[1]*State Key Laboratory of Advanced Optical Communication Systems and Networks,Department of Electronics, Beijing,*100871,*China;*
[2]*Institute of Electromagnetic Space,Southeast University,Nanjing,*210096,*China;*
[3]*State Key Laboratory of Millimeter Waves, Southeast University, Nanjing,*210096,*China;*
[4]*Pazhou Laboratory,Guangzhou,*510330,*China;*
[5]*Univ Rennes,CNRS,IETR-UMR 6164,Rennes,*F-35000,*France*

Appendix A Derivation of Eq. 1

We elaborate on the derivation of **Eq. 1** and provide necessary notations involved. For the SISO setting, the control coding pattern of the one-bit coding metasurface reads

$$\mathcal{C}_{m,n}^{SISO} = \text{sign}\left[\cos\left(\tilde{\phi}_{nm}^{SIIO}\right)\right] \tag{A1}$$

where $\tilde{\phi}_{nm}^{SISO} \equiv \tilde{\phi}_{m,n}\left(\boldsymbol{r}_q;\boldsymbol{r}_s\right), \tilde{\phi}_{m,n}\left(\boldsymbol{r}_q;\boldsymbol{r}_s\right) = \Delta_{m,n}\left(\boldsymbol{r}_q;\boldsymbol{r}_s\right) + \phi\left(\boldsymbol{r}_q\right)$,

$$\Delta_{m,n}\left(\boldsymbol{r}_q;\boldsymbol{r}_s\right) = k(\underbrace{|\boldsymbol{r}_s - \boldsymbol{r}_{m,n}|}_{R_{nm}(r_s)} + \underbrace{|\boldsymbol{r}_q - \boldsymbol{r}_{m,n}|}_{R_{nm}(r_q)}).$$

Herein, $\phi_q \equiv \phi\left(\boldsymbol{r}_q\right)(0 \leqslant \phi_q < 2\pi)$ denotes the intended phase directed from the source to receiver at $\boldsymbol{r}_q$ through the metasurface, and $\text{sign}(x)$ is the sign function:

$$\text{sign}(x) = \begin{cases} +1, x > 0 \\ 0, x = 0 \\ -1, x < 0 \end{cases}$$

Using the following identical equations:

$$\text{sign}(x) = \frac{-j}{\pi}\int_{-\infty}^{\infty}\frac{\exp(jx\xi)}{\xi}d\xi$$

$$\exp\left(j\xi\cos\left(\tilde{\phi}_{nm}\right)\right) = \sum_{p=-\infty}^{\infty}\exp\left(jp\tilde{\phi}_{nm}\right)j^p J_p(\xi)$$

we can express **Eq. A1** as:

$$\mathcal{C}_{m,n}^{SISO} = \frac{-j}{\pi}\int_{-\infty}^{\infty}\frac{1}{\xi}\sum_{p=-\infty}^{\infty}\exp\left(jp\tilde{\phi}_{nm}\right)j^p J_p(\xi)d\xi = \sum_{p=-\infty}^{\infty}B_p^{SISO}\exp\left(jp\tilde{\phi}_{nm}\right) \tag{A2}$$

where $B_p^{SISO} = \frac{-j^{p+1}}{\pi}\int_{-\infty}^{\infty}\frac{1}{\xi}J_p(\xi)d\xi = \frac{-j^{p+1}}{\pi}\int_{-\infty}^{\infty}\frac{1}{\xi}J_p(\xi)d\xi = \begin{cases}\frac{-j^{p+1}}{\pi}\cdot\frac{2}{p}, & p \text{ is odd} \\ 0, & \text{else}\end{cases}$. Now we can derive the radiation response of the one-bit coding metasurface as:

* Corresponding author (email: tjcui@seu.edu.cn, philipp.delhougne@gmail.com, lianlin.li@pku.edu.com)
† Shuang Y and Zhao H T have the same contribution to this work.

$$\begin{aligned}\widehat{\mathcal{H}}_{\mathrm{SISO}}\left(\mathbf{r},\mathbf{r}';q,s\right)&=\sum_{m,n}\mathcal{C}_{m,n}^{SISO}\cdot\frac{\exp\left[-j\Delta_{nm}\left(r;\mathbf{r}'\right)\right)]}{R_{nm}(\mathbf{r})R_{nm}\left(\mathbf{r}'\right)}\\&=\sum_{p=-\infty}^{\infty}B_1^{SISO}\exp\left(jp\phi_q\right)\sum_{m,n}\frac{\exp\left[jp\Delta_{m,n}\left(r_q;r_s\right)-j\Delta_{nm}\left(r;r'\right)\right)]}{R_{nm}(r)R_{nm}\left(r_s\right)}\\&=B_1^{SISO}\exp\left(j\phi_q\right)\underbrace{\sum_{m,n}\frac{\exp\left[j\Delta_{m,n}\left(r_q;r_s\right)-j\Delta_{nm}\left(r;\mathbf{r}'\right)\right)]}{R_{nm}(r)R_{nj}\left(\mathbf{r}'\right)}}_{A_1^{SISO}(r,r';q,q)}\\&+\sum_{p=-\infty,p\neq1}^{\infty}B_p^{SISO}\exp\left(jp\phi_q\right)\underbrace{\sum_{m,n}\frac{\exp\left[jp\Delta_{m,n}\left(r_q;r_s\right)-j\Delta_{nm}\left(r;\mathbf{r}'\right)\right)]}{R_{nm}\left(r_n\right)}}_{A_p^{SISO}(r,r';q,s')}\end{aligned}\tag{A3}$$

where $\sum_{m,n}\equiv\sum_{n=1}^{N}\sum_{m=1}^{M}$. After introducing the following notations

$$\begin{aligned}E_1^{SISO}\left(\boldsymbol{r},\mathbf{r}';q,s\right)&=B_1^{SISO}\exp\left(j\phi_q\right)A_1^{SISO}\left(\boldsymbol{r},\mathbf{r}';q,s\right)\\A_p^{SISO}\left(\boldsymbol{r},\mathbf{r}';q,s\right)&=\sum_{m,n}\frac{\exp\left[jp\Delta_{m,n}\left(r_q;\boldsymbol{r}_s\right)-j\Delta_{nm}\left(r;\mathbf{r}'\right)\right)]}{R_{nm}(\boldsymbol{r})R_{nm}\left(\mathbf{r}'\right)},\end{aligned}$$

then the proof of **Eq.1** in main text can be readily completed:

$$\widehat{\mathcal{H}}_{\mathrm{SISO}}\left(\mathbf{r},\mathbf{r}';q,s\right)=\underbrace{E_1^{\mathrm{SISO}}\left(\boldsymbol{r},\mathbf{r}';q,s\right)}_{\text{leading term}}+\underbrace{\sum_{p=-\infty,p\neq1}^{\infty}B_p^{SISO}A_p^{\mathrm{SISO}}\left(\boldsymbol{r},\mathbf{r}';q,s\right)\exp\left(jp\phi_q\right)}_{\text{perturbation terms}}\tag{A4}$$

Discussion 1. The derivation of $A_p=\frac{-j^{p+1}}{\pi}\int_{-\infty}^{\infty}\frac{1}{\xi}J_p(\xi)d\xi$.

We focus on the derivation of $A_p=\frac{-j^{p+1}}{\pi}\int_{-\infty}^{\infty}\frac{1}{\xi}J_p(\xi)d\xi$. It can be processed as

$$A_p=\frac{-j^{p+1}}{\pi}\int_{-\infty}^{\infty}\frac{1}{\xi}J_p(\xi)d\xi=\begin{cases}2\frac{-j^{p+1}}{\pi}\int_0^{\infty}\frac{1}{\xi}J_p(\xi)d\xi, & p\text{ is odd}\\0, & \text{else}\end{cases}=\begin{cases}-\frac{2}{p}\frac{j^{p+1}}{\pi}, & p\text{ is odd}\\0, & \text{is else}\end{cases}\tag{A5}$$

in which we have used a fundamental property of the Bessel function

$$J_p(-\xi)=(-1)^pJ_p(\xi)=J_{-p}(\xi)$$

and the integral identical equation of the Bessel function

$$\int_0^{\infty}\frac{1}{\xi}J_p(\xi)d\xi=\frac{1}{2}\frac{\Gamma\left(\frac{p}{2}\right)}{\Gamma\left(\frac{p}{2}+1\right)}=\frac{1}{p}\text{ if }p>0.$$

Discussion 2. Far-field solution of **Eq.A4**.

We study the system response $\widehat{\mathcal{H}}_{\mathrm{SISo}}$ when the source and receiver are in the far-field region of the one-bit coding metasurface. For this purpose, we would like to consider the calculation of $A_p^{SISO}\left(\boldsymbol{r},\boldsymbol{r}';q,s\right)$ in the spherical coordinate system. To this end, some necessary notations are introduced as follows:

$$\begin{aligned}&\hat{\boldsymbol{r}}_q=\hat{\boldsymbol{x}}\sin\left(\alpha_q\right)\cos\left(\beta_q\right)+\hat{\boldsymbol{y}}\sin\left(\alpha_q\right)\sin\left(\beta_q\right)+\hat{\mathbf{z}}\cos\left(\alpha_q\right),\\&\hat{\boldsymbol{r}}_s=\hat{\boldsymbol{x}}\sin\left(\alpha_s\right)\cos\left(\beta_s\right)+\hat{\boldsymbol{y}}\sin\left(\alpha_s\right)\sin\left(\beta_s\right)+\hat{\mathbf{z}}\cos\left(\alpha_s\right),\\&\hat{\boldsymbol{r}}=\hat{\boldsymbol{x}}\sin(\alpha)\cos(\beta)+\hat{\mathbf{y}}\sin(\alpha)\sin(\beta)+\hat{\mathbf{z}}\cos(\alpha),\\&\hat{\mathbf{r}}'=\hat{\boldsymbol{x}}\sin\left(\alpha'\right)\cos\left(\beta'\right)+\hat{\boldsymbol{y}}\sin\left(\alpha'\right)\sin\left(\beta'\right)+\hat{\mathbf{z}}\cos\left(\alpha'\right)\\&\boldsymbol{r}_{m,n}\cdot\left(\hat{\boldsymbol{r}}_q+\hat{\boldsymbol{r}}_s\right)=x_m\left[\sin\left(\alpha_q\right)\cos\left(\beta_q\right)+\sin\left(\alpha_s\right)\cos\left(\beta_s\right)\right]+\\&y_n\left[\sin\left(\alpha_q\right)\sin\left(\beta_q\right)+\sin\left(\alpha_s\right)\sin\left(\beta_s\right)\right],\\&\boldsymbol{r}_{m,n}\cdot\left(\hat{\boldsymbol{r}}+\hat{\boldsymbol{r}}'\right)=x_m\left[\sin(\alpha)\cos(\beta)+\sin\left(\alpha'\right)\cos\left(\beta'\right)\right]\\&+y_n\left[\sin(\alpha)\sin(\beta)+\sin\left(\alpha'\right)\sin\left(\beta'\right)\right],\\&\xi_p^{SISO}=\sin(\alpha)\cos(\beta)+\sin\left(\alpha'\right)\cos\left(\beta'\right)-p\left[\sin\left(\alpha_q\right)\cos\left(\beta_q\right)+\sin\left(\alpha_s\right)\cos\left(\beta_s\right)\right],\\&\eta_p^{SISO}=\sin(\alpha)\sin(\beta)+\sin\left(\alpha'\right)\sin\left(\beta'\right)-p\left[\sin\left(\alpha_q\right)\sin\left(\beta_q\right)+\sin\left(\alpha_s\right)\sin\left(\beta_s\right)\right].\end{aligned}$$

Then, $A_p^{SISO}\left(\boldsymbol{r},\boldsymbol{r}';q,s\right)$ under the far-field approximation can be derived as:

$$\begin{aligned}A_p^{SISO}\left(\boldsymbol{r},\boldsymbol{r}';q,s\right)&=\sum_{m,n}\frac{\exp\left[jp\Delta_{m,n}\left(r_q;\boldsymbol{r}_s\right)-j\Delta_{nm}\left(r;\mathbf{r}'\right)\right)]}{R_{nm}(\boldsymbol{r})R_{nm}\left(\mathbf{r}'\right)}\\&\approx\frac{\exp\left[jkp\left(r_q+r_s\right)-j\left(\left(r+r'\right)\right)\right]}{rr\prime}\sum_{m,n}\exp\left[-jkp\boldsymbol{r}_{m,n}\cdot\left(\hat{\boldsymbol{r}}_q+\hat{\boldsymbol{r}}_s\right)+jk\boldsymbol{r}_{m,n}\cdot\left(\hat{\boldsymbol{r}}+\hat{\boldsymbol{r}}'\right)\right]\\&\approx-\frac{\exp\left[jkp\left(r_q+r_s\right)-j\left(\left(r+r'\right)\right)\right]}{rr}L_xL_y\operatorname{sinc}\left(\frac{1}{2}kL_x\xi_p^{SISO}\right)\operatorname{sinc}\left(\frac{1}{2}kL_y\eta_p^{SISO}\right)\end{aligned}\tag{A6}$$

Here, L_x and L_y denote the scales of metasurface along the x - and y-directions, respectively; $\mathrm{sinc}(x) = \frac{\sin(x)}{x}$ has been defined; and the following approximation has been used

$$\Delta_{m,n}\left(\boldsymbol{r};\boldsymbol{r}'\right) = k\left(\left|\boldsymbol{r}'-\boldsymbol{r}_{m,n}\right| + \left|\boldsymbol{r}-\boldsymbol{r}_{m,n}\right|\right) \approx k\left(r'+r-\boldsymbol{r}_{m,n}\cdot\left(\hat{\boldsymbol{r}}+\hat{\boldsymbol{r}}'\right)\right) \tag{A7}$$

Using **Eq.A7** in **Eq.A4** immediately leads to the far-field expression of the system response for the SISO setting.

It is clear from **Eq.A6** that if the vector of $\hat{\boldsymbol{r}}+\hat{\boldsymbol{r}}'+\hat{\boldsymbol{r}}_q+\hat{\boldsymbol{r}}_s$ is along with the normal direction of the metasurface, then we have $\left|A_{-1}^{\mathrm{SIIO}}\right| = \left|A_1^{\mathrm{SISO}}\right|$. Recall that $B_{-1}^{\mathrm{SISO}} = B_1^{\mathrm{SISO}}$, we can arrive at the following conclusion: When the source and intended receiver are in the far-field region of the metasurface, the one-bit quantization of the metasurface can give rise to an unwanted dominant parasitic radiation beam

$$E_{\mathrm{parasite}}^{\mathrm{SISO}}\left(\boldsymbol{r},\mathbf{r}';q,s\right) = B_1^{\mathrm{SISO}}\exp\left(-j\phi_q\right)A_{-1}^{\mathrm{SISO}}\left(\boldsymbol{r},\mathbf{r}';q,s\right).$$

Note that this parasitic beam has the same maximum intensity as the desired radiation beam E_1^{SISO} but with different radiation phase shift $\exp\left(-j\phi_q\right)$. Please see more details about the parasitic radiation beams below.

Discussion 3. Parasitic radiation beams of the one-bit coding metasurface

We provide some insights into the parasitic radiation beams when the receiver and source fall into the far-field region of the one-bit coding metasurface. For convenience of discussion, we denote the location of the (m, n) meta-atom in the rectangular coordinate system by $\boldsymbol{r}_{m,n} = (nd_x, md_y, 0)$, where d_x and d_y are the scales of the meta-atom along the x - and y - directions, respectively. In term of the paraxial approximation, we have

$$\left|\boldsymbol{r}-\boldsymbol{r}_{m,n}\right| \approx z + \frac{\rho^2+\rho_{mn}^2-2\left(nd_x\rho_x+md_y\rho_y\right)}{2z} \tag{A8}$$

Herein, $r=(\rho_x,\rho_y,z)$, $\rho^2=\rho_x^2+\rho_y^2$ and $\rho_{mn}^2=(nd_x)^2+(md_y)^2$. Note that one of the critical issues for calculating A_p^{SISO} is to deal with $p\Delta_{nm}\left(\boldsymbol{r}_q;\boldsymbol{r}_s\right)-\Delta_{nm}\left(\boldsymbol{r};\boldsymbol{r}'\right)$. To that end, we apply the paraxial approximation to $\Delta_{nm}\left(\boldsymbol{r};\boldsymbol{r}'\right)$ and $\Delta_{nm}\left(\boldsymbol{r}_q;\boldsymbol{r}_s\right)$, in particular,

$$\begin{aligned}\Delta_{nm}\left(\boldsymbol{r};\boldsymbol{r}'\right) &= k\left|\boldsymbol{r}'-\boldsymbol{r}_{m,n}\right| + k\left|\boldsymbol{r}-\boldsymbol{r}_{m,n}\right| \\ &\approx k\left(z'+z\right) + k\frac{\rho'^2+\rho_{mn}^2-2\left(nd_x\rho_x'+md_y\rho_y'\right)}{2z'} + k\frac{\rho^2+\rho_{mn}^2-2\left(nd_x\rho_x+md_y\rho_y\right)}{2z}\end{aligned} \tag{A9}$$

and

$$\begin{aligned}\Delta_{nm}\left(\boldsymbol{r}_q;\boldsymbol{r}_s\right) &= k\left|\boldsymbol{r}_s-\boldsymbol{r}_{m,n}\right| + k\left|\boldsymbol{r}_q-\boldsymbol{r}_{m,n}\right| \\ &\approx k\left(z_s+z_q\right) + k\frac{\rho_s^2+\rho_{mn}^2-2\left(nd_x\rho_{sx}+md_y\rho_{sy}\right)}{2z_s} + k\frac{\rho_q^2+\rho_{mn}^2-2\left(nd_x\rho_{qx}+md_y\rho_{qy}\right)}{2z_q}.\end{aligned} \tag{A10}$$

Then, $p\Delta_{nm}\left(\boldsymbol{r}_q;\boldsymbol{r}_s\right)-\Delta_{nm}\left(\boldsymbol{r};\boldsymbol{r}'\right)$ becomes:

$$\begin{aligned}&p\Delta_{nm}\left(\boldsymbol{r}_q;\boldsymbol{r}_s\right)-\Delta_{nm}\left(\boldsymbol{r};\boldsymbol{r}'\right) = pk\frac{\rho_{mn}^2-2\left(nd_x\rho_{sx}+md_y\rho_{sy}\right)}{2z_s} + pk\frac{\rho_{mn}^2-2\left(nd_x\rho_{qx}+md_y\rho_{qy}\right)}{2z_q} \\ &-k\frac{\rho_{mn}^2-2\left(nd_x\rho_x'+md_y\rho_y'\right)}{2z'} - k\frac{\rho_{mn}^2-2\left(nd_x\rho_x+md_y\rho_y\right)}{2z} + k\cdot\varepsilon^{SISO} \\ &= -\frac{k}{2z}\underbrace{\left(1+\frac{z}{z'}-p\frac{z}{z_s}-p\frac{z}{z_q}\right)}_{\beta^{SISO}}\rho_{mn}^2 + \underbrace{\left(\rho_x+\frac{z}{z'}\rho_x'-\frac{z}{z_s}p\rho_{sx}-\frac{z}{z_q}p\rho_{qx}\right)}_{\frac{k}{z}}nd_x \\ &+\frac{k}{z}\underbrace{\left(\rho_y+\frac{z}{z'}\rho_y'-\frac{z}{z_s}p\rho_{sy}-\frac{z}{z_q}p\rho_{qy}\right)}_{b_y^{SISO}}md_y + k\cdot\mathcal{E}^{SISO}\end{aligned} \tag{A11}$$

Herein, $\mathcal{E}^{\mathrm{SISO}} = p\left(z_s+z_q\right)-\left(z'+z\right)+p\left(\frac{\rho_S^2}{2z_s}+\frac{\rho_q^2}{2z_q}\right)-\left(\frac{\rho'^2}{2z'}+\frac{\rho^2}{2z}\right)$, $\boldsymbol{r}_s=(\rho_{sx},\rho_{sy},z_s)$ $\rho_s^2=\rho_{sx}^2+\rho_{sy}^2$, $\boldsymbol{r}_q=(\rho_{qx},\rho_{qy},z_q)$, $\rho_q^2=\rho_{qx}^2+\rho_{qy}^2$. Substituting **Eq. A11** into $A_p^{SISO}\left(\boldsymbol{r},\boldsymbol{r}';q,s\right)$, leads to:

$$\begin{aligned}A_p^{SISO}\left(\boldsymbol{r},\boldsymbol{r}';q,S\right) &= \sum_{m,n}\frac{\exp\left[j\left(p\Delta_{nm}\left(\boldsymbol{r}_q;\boldsymbol{r}_S\right)-\Delta_{nm}\left(\boldsymbol{r};\boldsymbol{r}'\right)\right)\right]}{R_{nm}(\boldsymbol{r})R_{nm}(\boldsymbol{r}\prime)} \\ &\approx \frac{1}{zZ'}\frac{\pi}{\alpha+i\frac{k\beta^{SISO}}{2z}}\exp\left(-\frac{k^2}{4z^2}\frac{\left(b_x^{SISO}\right)^2+\left(b_y^{SISO}\right)^2}{\alpha+i\frac{k\beta^{SISO}}{2z}}\right)\exp\left(jk\mathcal{E}^{SISO}\right)\end{aligned} \tag{A12}$$

In the second line of **Eq**.**A12**, we have assumed the Gaussian illumination beam of the source, and the beam width is $\alpha = (Nd_x/2)^{-2}$. In addition, the following integral identical equation has been used

$$\int_{-\alpha}^{\alpha}\exp\left(-\alpha t^2+j\beta t^2+jbt\right)dt = \sqrt{\frac{\pi}{\alpha-i\beta}}\exp\left(-\frac{b^2}{4(\alpha-i\beta)}\right)$$

It is clear from Eq. A12 that the parasitic beams of the one-bit coding metasurface can be observed at $(\rho_x(p),\rho_y(p),z)$ $(p=-1,\pm3,\pm5,\ldots)$, where ρ_x and ρ_y are defined as

$$\rho_x(p,z) = \frac{z}{z_s}p\rho_{sx}+\frac{z}{z_q}p\rho_{qx}-\frac{z}{z'}\rho_x' \tag{A13}$$

$$\rho_y(p,z) = \frac{z}{z_s}p\rho_{sy}+\frac{z}{z_q}p\rho_{qy}-\frac{z}{z'}\rho_y' \tag{A14}$$

Appendix B Some details about Fig. 2

We here provide details about $\left|E_p^{\mathrm{SISO}}\right|$ involved in Fig. 2 in the main text. **Fig. B1** plots the spatial maps of $\left|\widehat{\mathcal{H}}_{\mathrm{SISO}}\right|$ corresponding to **Fig. 2** in the main text. In order to show details of $\left|E_p^{\mathrm{SISO}}\right|$, the first a few non-zero terms $\left|E_p^{SISO}\right|$ are normalized by their maximum. From these figures, we can verify two findings made in the main text, i.e., 1) the quantization energy loss is statistically uniformly distributed over the entire space when the receiver or/and source is in the near-field region of the metasurface; and 2) multiple unwanted parasitic beams appear that interfere with the desired beam when the receiver and source are in the far-field region of the one-bit coding metasurface.

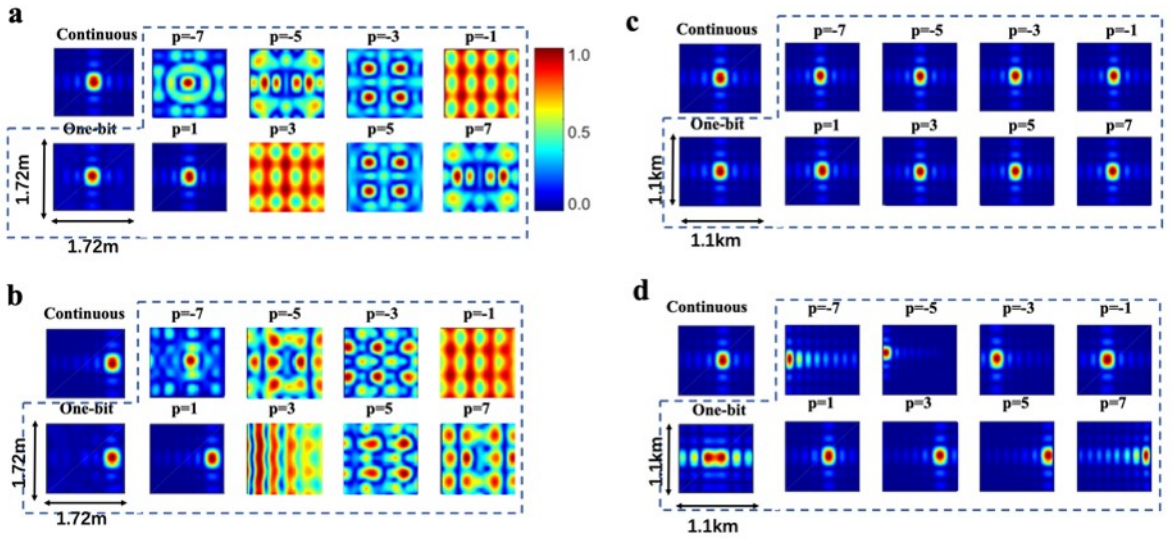

Figure B1 Spatial maps of $\left|\widehat{\mathcal{H}}_{\mathrm{SISO}}\right|$ for continuous and one-bit coding metasurfaces. The simulation setup and notations are the same as those in Fig.2 in main text, but the maps of $\left|E_p^{SISO}\right|$ are normalized by their own maximum.

Appendix C Derivation of Eq. 7

We elaborate on the derivation of **Eq.7** in the main text. For the SIMO setting, the control coding pattern of the one-bit coding metasurface reads

$$\mathcal{C}_{m,n}^{SIMO} = \mathrm{sign}\left[\sum_{q=1}^{Q}\cos\left(\tilde{\phi}_{nm}^{SIMO}(q)\right)\right] \tag{C1}$$

where $\tilde{\phi}_{nm}^{SIMO}(q) \equiv \tilde{\phi}_{m,n}\left(\boldsymbol{r}_q;\boldsymbol{r}_s\right)$, $\tilde{\phi}_{m,n}\left(\boldsymbol{r}_q;\boldsymbol{r}_s\right) = \Delta_{m,n}\left(\boldsymbol{r}_q;\boldsymbol{r}_s\right)+\phi_q$, and $\Delta_{m,n}\left(\boldsymbol{r}_q;\boldsymbol{r}_s\right) = k(\underbrace{|\boldsymbol{r}_s-\boldsymbol{r}_{m,n}|}_{R_{nm}(r_s)}+\underbrace{|\boldsymbol{r}_q-\boldsymbol{r}_{m,n}|}_{R_{nm}(r_q)})$. Similar to those in Appendix A, we express **Eq. C1** as:

$$\begin{aligned}
\mathcal{C}_{m,n}^{SIMO} &= \mathrm{sign}\left[\sum_{q=1}^{Q}\cos\left(\tilde{\phi}_{nm}^{SIMO}(q)\right)\right] = \frac{-j}{\pi}\int_{-\infty}^{\infty}\frac{1}{\xi}\prod_{q=1}^{Q}\exp\left[j\xi\cos\left(\tilde{\phi}_{nm}(q)\right)\right]d\xi \\
&= \frac{-j}{\pi}\int_{-\infty}^{\infty}\frac{1}{\xi}\sum_{p_1}\sum_{p_2}\cdots\sum_{p_Q}\exp\left(j\sum_{q}p_q\tilde{\phi}_{nm}(q)\right)j^{\Sigma_q p_q}\prod_{q=1}^{Q}J_{p_q}(\xi)d\xi \\
&= \sum_{p_1}\sum_{p_2}\cdots\sum_{p_Q}\exp\left(j\sum_{q}p_q\tilde{\phi}_{nm}(q)\right)\int_{-\infty}^{\infty}\frac{-j}{\pi}j^{2\Sigma_q p_q}\frac{1}{\xi}\prod_{q=1}^{Q}J_{p_q}(\xi)d\xi
\end{aligned} \tag{C2}$$

in which, $\sum_{p_i} \equiv \sum_{p_i=-\infty}^{\infty}$ and $\sum_q \equiv \sum_{q=1}^{Q}$. After introducing the notations $B_{\{p_i\}}^{SMO} \equiv \frac{-j}{\pi}j^{\Sigma_q p_q}\int_{-\infty}^{\infty}\frac{1}{\xi}\Pi_{q=1}^{Q}J_{p_q}(\xi)d\xi$ and $\Sigma_{\{p_i\}} \equiv \sum_{p_1}\Sigma_{p_2}\cdots\Sigma_{p_Q}$, we can express **Eq.C2** as:

$$\mathcal{C}_{m,n}^{SIMO} = \sum_{\{p_i\}}B_{\{p_i\}}^{SIMO}\exp\left(j\sum_{q}p_q\tilde{\phi}_{nm}(q)\right) \tag{C3}$$

Now, we can arrive at the SIMO's system response of the one-bit coding metasurface as

$$\begin{aligned}
\widehat{\mathcal{H}}_{\text{SIMO}}\ (\mathbf{r},\mathbf{r}';\{q\},s) &= \sum_{m,n}\mathcal{C}_{m,n}^{SIMO}\frac{\exp\left[-j\Delta_{nm}\left(r;\mathbf{r}'\right)\right)]}{R_{nm}(r)R_{nm}\left(\mathbf{r}'\right)} \\
&= \sum_{\{p_i\}}\exp\left(j\sum_q p_q\phi_q\right)B_{\{p_i\}}^{\text{SIMO}}\underbrace{\sum_{m,n}\frac{\exp\left[j\Sigma_q p_q\Delta_{m,n}\left(r_q;\mathbf{r}_s\right)-j\Delta_{nm}\left(r;\mathbf{r}'\right)\right)]}{R_{nm}(r)r_{nm})}}_{A_{\{p_i\}}^{SIM}(r,\mathbf{r}')} \\
&= \underbrace{B_1^{\text{SIMO}}\sum_{q=1}^{Q}\exp\left(j\phi_q\right)A_1^{SISO}\left(\boldsymbol{r},\mathbf{r}';q,s\right)}_{E_1^{SIMO}(r,\mathbf{r}';\{q\},s)}+ \\
&+\underbrace{\sum_{\{p_i\}/\{\sum_i|p_i|=1\&p_i\neq-1\}}E_{\{p_{ij}\}}^{SIMO}\left(\boldsymbol{r},\mathbf{r}';\{q\},s\right)\exp\left[j\sum_{q=1}^{Q}p_q\phi_q\right]}_{\text{perturbation terms}}
\end{aligned} \tag{C4}$$

Herein, $B_1^{SIMO}=\frac{1}{\pi}\int_{-\infty}^{\infty}\frac{1}{\xi}J_1(\xi)J_0^{Q-1}(\xi)d\xi$, and $E_{\{p_{ij}\}}^{SIMO}\left(\boldsymbol{r},\mathbf{r}';\{q\},s\right)=B_{\{p_i\}}^{SIMO}A_{\{p_i\}}^{SIMO}\left(\boldsymbol{r},\mathbf{r}'\right)$. In addition, the operator denoted by $\sum_{\{p_i\}/\{\sum_i|p_i|=1\&p_i\neq-1\}}$ is defined as follows. For a function of $f\left(p_1,p_2,\ldots,p_Q\right)$, we define:

$$\sum_{\{p_i\}/\{\sum_i|p_i|=1\&p_i\neq-1\}}f\left(p_1,p_2,\ldots,p_Q\right)=\sum_{\{p_i\}}f\left(p_1,p_2,\ldots,p_Q\right)-\left[f(1,0,0,\ldots,0)+f(0,1,0,\ldots,0)+\cdots+f(0,0,0,\ldots,1)\right]$$

Discussion 1. The derivation of $B_{\{p_1,p_2\}}^{SIMO}=\frac{-jp_1+p_2+1)}{\pi}\int_{-\infty}^{+\infty}\frac{J_{p_1}(\xi)p_{p_2}(\xi)}{\xi}d\xi$.

We consider the calculation of $B_{\{p_i\}}^{SIMO}$ for the special SIMO case: single-input double-output, Q=2. Then, we deal with $B_{\{p_1,p_2\}}^{SIMO}=\frac{-j(p_1+p_2+1)}{\pi}\int_{-\infty}^{+\infty}\frac{J_{p_1}(\xi)J_{p_2}(\xi)}{\xi}d\xi$ as follows:

$$\begin{aligned}
B_{\{p_1,p_2\}}^{\text{SIMO}} &= \frac{-j^{(p_1+p_2+1)}}{\pi}\int_{-\infty}^{+\infty}\frac{J_{p_1}(\xi)J_{p_2}(\xi)}{\xi}d\xi \\
&= \frac{-jp_1+p_2+1)}{\pi}\cdot\frac{2}{\pi}\int_{-\infty}^{\infty}\int_0^{\frac{\pi}{2}}\frac{J_{p_1+p_2}(2x\cos\theta)\cos\left[\left(p_1-p_2\right)\theta\right]}{\xi}d\theta d\xi \\
&= \frac{-j^{(p_1+p_2+1)}}{\pi}\cdot\frac{2}{\pi}\int_0^{\frac{\pi}{2}}\cos\left[\left(p_1-p_2\right)\theta\right]\left[\int_{-\infty}^{\infty}\frac{J_{p_1+p_2}(2x\cos\theta)}{\xi}d\xi\right]d\theta \\
&= \frac{-j^{(p_1+p_2+1)}}{\pi}\cdot\frac{2}{\pi}\cdot\frac{2}{p_1+p_2}\int_0^{\frac{\pi}{2}}\cos\left[\left(p_1-p_2\right)\theta\right]d\theta \\
&= \frac{-j\left(p_1+p_2+1\right)}{p_1+p_2}\cdot\left(\frac{2}{\pi}\right)^2\cdot\frac{\sin\left[\left(p_1-p_2\right)\frac{\pi}{2}\right]}{p_1-p_2}
\end{aligned} \tag{C5}$$

In the first and fourth lines of **Eq. C5**, the following identical equations

$$J_{p_1}(x)J_{p_2}(x)=\frac{2}{\pi}\int_0^{\frac{\pi}{2}}J_{p_1+p_2}(2x\cos\theta)\cos\left[\left(p_1-p_2\right)\theta\right]d\theta,$$

$$\int_{-\infty}^{\infty}\frac{J_{p_1+p_2}(2\xi\cos\theta)}{\xi}d\xi=\begin{cases}0, & p_1+p_2 \text{ is even}\\ \frac{2}{p_1+p_2}, & p_1+p_2 i \text{ is odd}\end{cases}$$

have been used, respectively. Finally, we can arrive at the closed-form solution of $B_{\{p_1,p_2\}}^{SIO}$ as

$$B_{\{p_1,p_2\}}^{SIMO}=\begin{cases}0, & p_1+p_2 \text{ is even}\\ \frac{-j(p_1+p_2+1)}{p_1+p_2}\cdot\left(\frac{2}{\pi}\right)^2\cdot\frac{\sin\left[\left(p_1-p_2\right)\frac{\pi}{2}\right]}{p_1-p_2}, & p_1+p_2 \text{ is odd}\end{cases} \tag{C6}$$

Especially, the leading term is $B_0^{SIMO}=\frac{2}{\pi}\int_0^{\infty}\frac{1}{\xi}J_0(\xi)J_1(\xi)d\xi=\left(\frac{2}{\pi}\right)^2$.

Discussion 2. Parasitic radiation beams of the one-bit coding metasurface

We here provide some insights into the parasitic radiation beams when the source and multiple intended receivers are deployed

in the far-field region of the one-bit coding metasurface. Similar to above, we treat $\sum_q p_q \Delta_{nm}(\boldsymbol{r}_q;\boldsymbol{r}_s) - \Delta_{nm}(\boldsymbol{r};\boldsymbol{r}')$ as follows:

$$\begin{aligned}\sum_q p_q \Delta_{nm}(\boldsymbol{r}_q;\boldsymbol{r}_s) - \Delta_{nm}(\boldsymbol{r};\boldsymbol{r}') = &-\underbrace{\frac{k}{2z}\left(1+\frac{z}{z'}-\sum_q p_q\left(\frac{z}{z_s}+\frac{z}{z_q}\right)\right)}_{\beta^{\mathrm{SIMO}}}\rho_{mn}^2 \\ &+\underbrace{\frac{k}{z}\left(\rho_x+\frac{z}{z'}\rho_x'-\sum_q p_q\left(\frac{z}{z_s}\rho_{sx}+\frac{z}{z_q}\rho_{qx}\right)\right)}_{b_x^{\mathrm{SIMO}}} nd_x \\ &+\underbrace{\frac{k}{z}\left(\rho_y+\frac{z}{z'}\rho_y'-\sum_q p_q\left(\frac{z}{z_s}\rho_{sy}+\frac{z}{z_q}\rho_{qy}\right)\right)}_{b_y^{\mathrm{SIMO}}} md_y + k\mathcal{E}^{\mathrm{SIMO}}\end{aligned}$$

Herein, $\varepsilon^{SIMO} = p(z_s+z_q) - (z'+z) + \sum_q p_q\left(\frac{\rho_s^2}{2z_s}+\frac{\rho_q^2}{2z_q}\right) - \left(\frac{\rho'^2}{2z'}+\frac{\rho^2}{2z}\right)$. Along the same line as that used in **Appendix A**, we can arrive at the close-form solution to $A_{\{p_i\}}^{SMO}(\boldsymbol{r},\boldsymbol{r}';\{q\},s)$:

$$\begin{aligned}A_{\{p_i\}}^{\mathrm{SIMO}}(\boldsymbol{r},\boldsymbol{r}';\{q\},s) &= \sum_{m,n}\frac{\exp\left(j\left[\sum_{q=1}^{Q} p_q\Delta_{m,n}(r_q;r_s) - \Delta_{m,n}(r;rr')\right]\right)}{R_{nm}(\boldsymbol{r})R_{nm}(r')} \\ &\approx \frac{1}{zz\prime}\frac{\pi}{\alpha+i\frac{k\beta^{\mathrm{SIMO}}}{2z}}\exp\left(-\frac{k^2}{4z^2}\frac{\left(b_x^{\mathrm{SIMO}}\right)^2+\left(b_y^{\mathrm{SIMO}}\right)^2}{\alpha+i\frac{k\beta^{\mathrm{SIMO}}}{2z}}\right)\exp\left(jk\mathcal{E}^{\mathrm{SIMO}}\right).\end{aligned} \tag{C7}$$

Then, for the SIMO setting, the parasitic radiation beams can be observed at the locations of $(\rho_x(\{p_q\}), \rho_y(\{p_q\}), z)$, where $\rho_x(\{p_q\}) = \sum_q p_q\left(\frac{z}{z_s}\rho_{sx}+\frac{z}{z_q}\rho_{qx}\right) - \frac{z}{z'}\rho_x'$, and $\rho_y(\{p_q\}) = \sum_q p_q\left(\frac{z}{z_s}\rho_{sy}+\frac{z}{z_q}\rho_{qy}\right) - \frac{z}{z'}\rho_y'$.

Discussion 3. Far-field solution of **Eq. C4**

Here, we will study the system response $\widehat{\mathcal{H}}_{\mathrm{SIM}}$ when the source and intended receivers are in the far-field region of the one-bit coding metasurface. Similar to the SISO case discussed in **Appendix A**, we deal with $A_{\{p_i\}}^{SIO}(\boldsymbol{r},\boldsymbol{r}';\{q\},s)$ as follows

$$\begin{aligned}A_{\{p_i\}}^{SIMO}(\boldsymbol{r},\boldsymbol{r}';\{q\},s) \approx &\frac{\exp\left[jk\sum_q p_q(r_q+r_s) - jk((r+r'))\right]}{rr'} \\ &\times\sum_{m,n}\exp\left[-jk\boldsymbol{r}_{m,n}\cdot\sum_q p_q(\hat{\boldsymbol{r}}_q+\hat{\boldsymbol{r}}_s) + jk\boldsymbol{r}_{m,n}\cdot(\hat{\boldsymbol{r}}+\hat{\boldsymbol{r}}')\right] \\ \approx &-\frac{\exp\left[jk\sum_q p_q(r_q+r_s) - jk((r+r'))\right]}{rr'} \\ &\times L_xL_y\,\mathrm{sinc}\left(\frac{1}{2}kL_x\xi^{\mathrm{SIMO}}(\{p_i\})\right)\mathrm{sinc}\left(\frac{1}{2}kL_y\eta^{\mathrm{SIMO}}(\{p_i\})\right)\end{aligned} \tag{C8}$$

Herein, ξ^{SIMO} and η^{SIMO} are defined as: $\xi^{\mathrm{SIMO}}(\{p_i\}) = \sin(\alpha)\cos(\beta) + \sin(\alpha')\cos(\beta') - \sum_q p_q[\sin(\alpha_q)\cos(\beta_q) + \sin(\alpha_s)\cos(\beta_s)]$, and $\eta^{\mathrm{SIMO}}(\{p_i\}) = \sin(\alpha)\sin(\beta) + \sin(\alpha')\sin(\beta') - \sum_q p_q[\sin(\alpha_q)\sin(\beta_q) + \sin(\alpha_s)\sin(\beta_s)]$, respectively. It is noted that the farfield approximation is explicitly used in the second line of **Eq. C8**. It is readily observed from **Eq. C8** that the parasitic radiation beams can be observed when the vector of $\sum_q p_q(\hat{\boldsymbol{r}}_q+\hat{\boldsymbol{r}}_s)+\hat{\boldsymbol{r}}+\hat{\boldsymbol{r}}$ is perpendicular to the normal of the one-bit coding metasurface, and these unwanted parasitic beams are described by the perturbation terms of **Eq. C4** :

$$B_1^{SIMO}\exp(-j\phi_q)\,A_{\{p_i\}}^{SIMO}(r,\boldsymbol{r}';\{q\},s),(q=1,2,\ldots,Q).$$

Discussion 4. The efficiency of the closed-form expression $\mathcal{C}_{m,n}^{SIMO}$

As an additional set of examinations for **Figs. 4** and **5** in the main text, we validate our closed-form solution in designing the desired radiation pattern of the one-bit coding metasurface. As an illustrative example, we consider the SIMO case with Q = 3, and thus $\mathcal{C}_{m,n}^{SIMO}$ is concerned. To this end, we study the performance of the modified Gerchberg-Saxton (G-S) algorithm [32] initialized with the result by $\mathcal{C}_{m,n}^{SIMO}$. **Figure C1(a)** plots the evolution behavior of the intensities at three intended receivers with growing iteration. **Figure C1(b)** show spatial maps of $\left|\widehat{\mathcal{H}}_{\mathrm{SISO}}\right|$ of the onebit coding metasurface for three different iteration steps (iteration=1,5 and 10). Note that the result of $\left|\widehat{\mathcal{H}}_{SISO}\right|$ with iteration=1 is just the result using our formula $\mathcal{C}_{m,n}^{SIMO}$. This set of figures show that no obvious improvement is observed by using the iterative GS algorithm when it is initialized by our simple formula. That is to say, the proposed formula for obtaining the coding pattern of the one-bit coding metasurface, $\mathcal{C}_{m,n}^{SIMO}$, yields satisfactory results of a quality comparable to that achieved with the iterative G-S algorithm.

Discussion 5. Approximating the system response of the continuous metasurface with that of a one-bit coding metasurface

We investigate the relation of the system response between the ideal and one-bit coding metasurface from the viewpoint outlined by **Eq. 8** in main text. For illustrative purposes, we here consider the SIMO case. **Figure C2(a)** reports the map of the approximate error (relative RMSE) for varying Q and K. A red dash-dotted line indicates the contour on which the relative RMSE is 0.2. We denote with $K_{0.2}(Q)$ the value of K at a given Q for which the relative RMSE is 0.2. In **Figure C2(b)**, we compare the dependence of $K_{0.2}$ and $Q/\gamma_{\text{one-bit}}$ on the number of channels Q. It is clear that the system response of the ideal metasurface can be well approximated by using K responses of the one-bit coding metasurface which can be achieved by using one one-bit programmable metasurface with K well-designed control coding patterns.

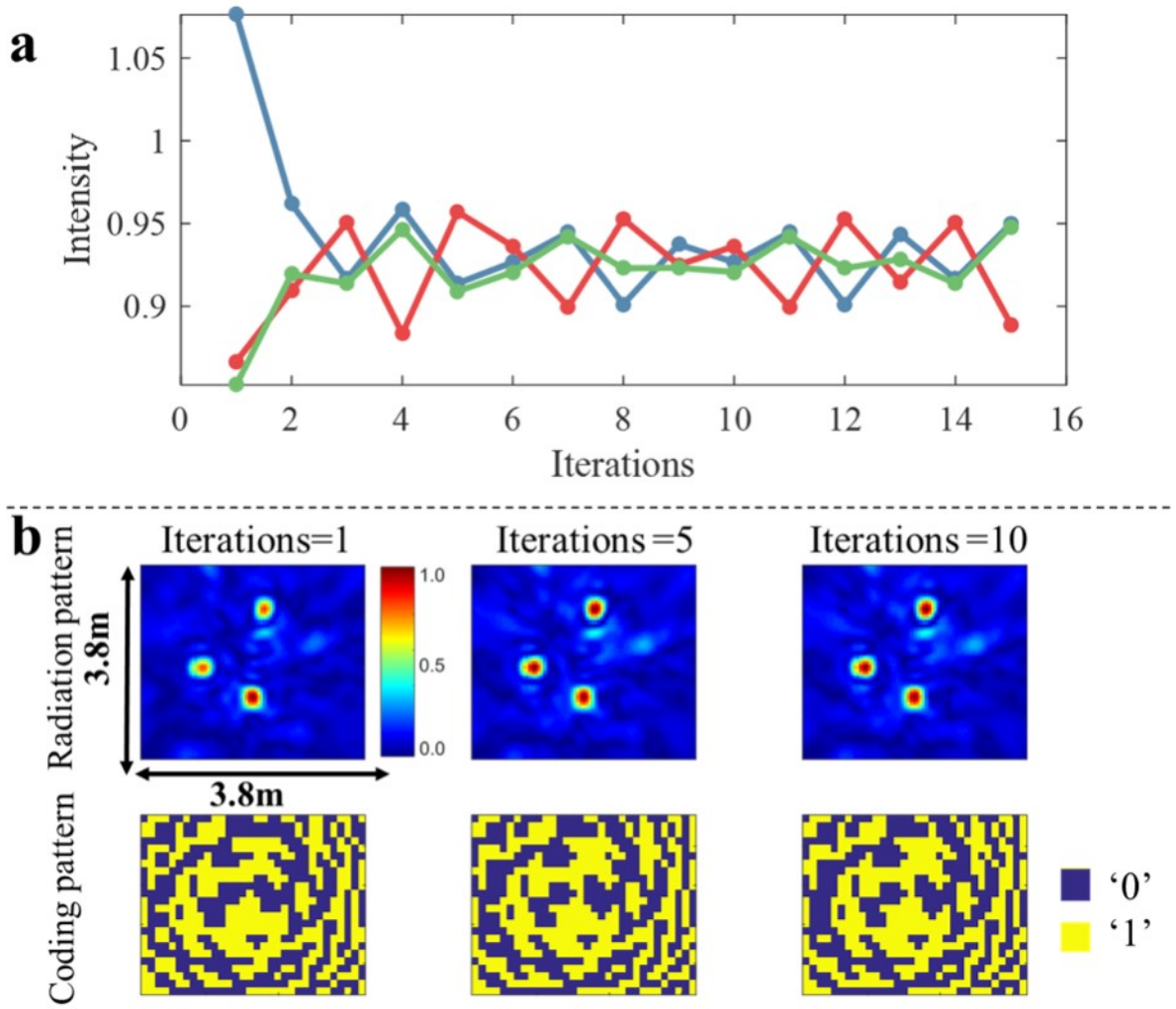

Figure C1 **a**. The evolution behavior of the intensities at three intended receivers with the growth of iteration. **b**. Spatial maps of $\left|\widehat{\mathcal{H}}_{\mathrm{SISO}}\right|$ for three different iteration steps, i.e., iteration=1,5 and 10. Note that the result of $\left|\widehat{\mathcal{H}}_{SISO}\right|$ with iteration=1 is just the result by using our formula $\mathcal{C}_{m,n}^{SIMO}$. Here, the resultant coding patterns of the one-bit coding metasurface have also been provided.

Appendix D Derivation of the MIMO's system response

We here elaborate on the derivation of the MIMO's system response of the one-bit metasurface. In this case, the coding pattern of the one-bit coding pattern reads:

$$\mathcal{C}_{m,n}^{MIMO} = \mathrm{sign}\left[\sum_{s=1}^{S}\sum_{q_s=1}^{Q_s}\cos\left(\tilde{\phi}_{nm}^{MIMO}\left(q_s\right)\right)\right] \tag{D1}$$

where $\tilde{\phi}_{nm}^{MIMO}\left(q_s\right) \equiv \tilde{\phi}_{m,n}\left(\boldsymbol{r}_q;\boldsymbol{r}_s\right), \tilde{\phi}_{m,n}\left(\boldsymbol{r}_q;\boldsymbol{r}_s\right) = \Delta_{m,n}\left(\boldsymbol{r}_q;\boldsymbol{r}_s\right) + \phi_{q_s}$, and $\Delta_{m,n}\left(\boldsymbol{r}_q;\boldsymbol{r}_s\right) = k(\underbrace{|\boldsymbol{r}_s - \boldsymbol{r}_{m,n}|}_{R_{nm}(r_s)} + \underbrace{|\boldsymbol{r}_q - \boldsymbol{r}_{m,n}|}_{R_{nm}(r_q)})$.

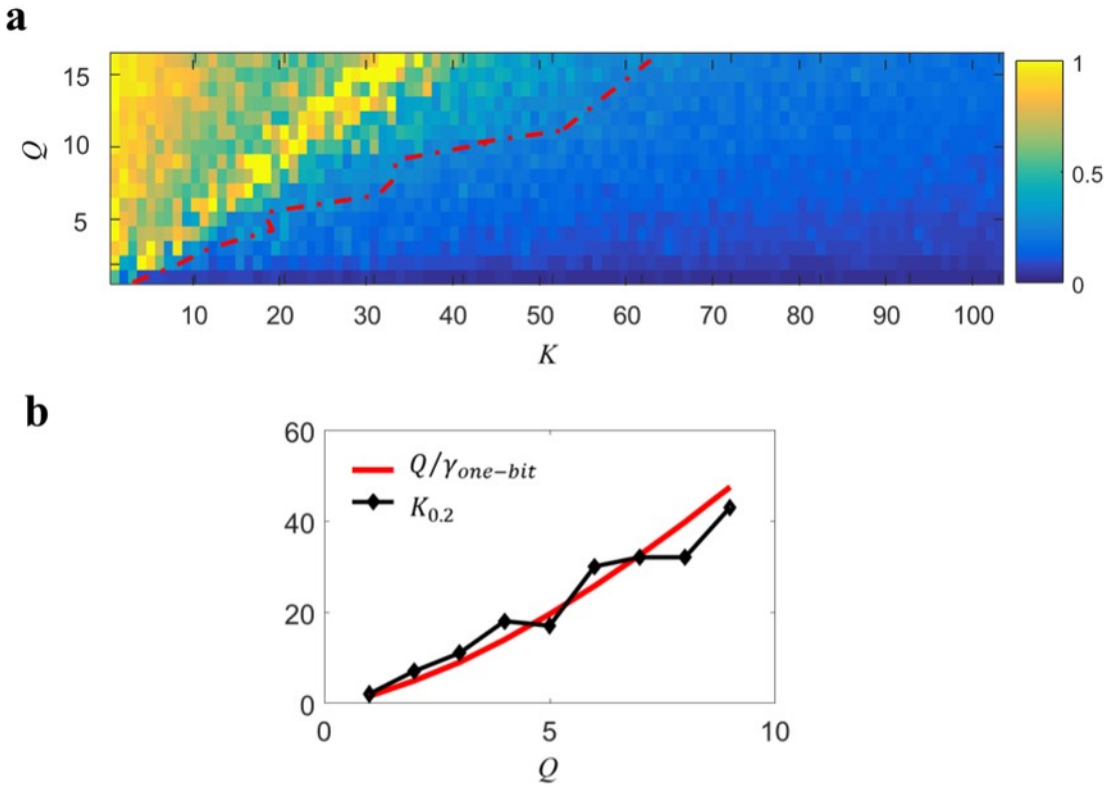

Figure C2 The relation of the system responses for continuous and one-bit coding metasurfaces. **a**. Map of relative RMSE using K well-designed system responses of the one-bit coding metasurface to approximate that of the continuous coding metasurface. The red line indicates the contour at which the relative RMSE is 0.2. **b**. Comparison of the dependence of $K_{0.2}$ and $Q/\gamma_{\text{one-bit}}$ on the number of channels Q.$K_{0.2}$ denotes the value of K when the approximate RMSE is 0.2 (see red dash-dotted line in **a**.

Along the same line as that in Appendix **A** and **C**, we can express **Eq. D1** as follows

$$
\begin{aligned}
\mathcal{C}_{m,n}^{SIMO} &= \text{sign}\left[\sum_{s=1}^{S}\sum_{q_s=1}^{Q_S}\cos\left(\tilde{\phi}_{nm}^{MIMO}\right)\right] = \frac{-j}{\pi}\int_{-\infty}^{\infty}\frac{1}{\xi}\prod_{s=1}^{S}\prod_{q_s=1}^{Q_S}\exp\left[j\xi\cos\left(\tilde{\phi}_{m,n}\right)\right]d\xi \\
&= \frac{-j}{\pi}\int_{-\infty}^{\infty}\frac{1}{\xi}\sum_{\{p_{q_s}\}} j^{\sum_{\{q_s\}} p_{q_s}}\exp\left(j\sum_{\{q_s\}} p_{q_s}\tilde{\phi}_{nm}\right)\prod_{\{q_s\}} J_{p_{q_s}}(\xi)d\xi \\
&= \sum_{\{p_{q_s}\}}\exp\left(j\sum_{\{q_s\}} p_{q_s}\tilde{\phi}_{nm}\right)\underbrace{\frac{-j}{\pi}\int_{-\infty}^{\infty}\frac{1}{\xi}j_{\{q_s\}}p_{q_s}\prod_{\{q_s\}} J_{p_{q_s}}(\xi)d\xi}_{B_{\{q_{q_s}\}}^{MiMO}} \\
&= \sum_{\{p_{q_s}\}} B_{\{p_{q_s}\}}^{MIMO}\exp\left(j\sum_{\{q_s\}} p_{q_s}\tilde{\phi}_{nm}\right)
\end{aligned}
\tag{D2}
$$

Herein, $\sum_{\{p_{q_s}\}} \equiv \underbrace{\sum_{p_{1_1}}\sum_{p_{2_1}}\cdots\sum_{Q_{Q_1}}}_{s=1}\underbrace{\sum_{p_{1_2}}\sum_{p_{2_2}}\cdots\sum_{p_{Q_2}}}_{s=2}\cdots\underbrace{\sum_{p_{1_S}}\sum_{p_{2_S}}\cdots\sum_{p_{Q_S}}}_{s=s}$, $\sum_{p_{q_s}} = \sum_{q_{q_s}=-\alpha}^{\alpha}$, $\sum_{\{q_s\}} \equiv \sum_{s=1}^{S}\sum_{q_s=1}^{Q_s}$,and $\prod_{\{q_s\}} \equiv$

$\prod_{s=1}^{S}\prod_{q_s=1}^{Q_s}$. Then the MIMO's system response of the one-bit coding metasurface can be derived as

$$\begin{aligned}\widehat{\mathcal{H}}_{\text{MIMO}}\ (\mathbf{r},\mathbf{r}';\{q_s\}) &= \sum_{m,n}\mathcal{C}_{m,n}^{MIMO}\frac{\exp\left[-j\Delta_{nm}\left(r;\mathbf{r}'\right)\right)]}{R_{nm}(\mathbf{r})R_{nm}\left(\mathbf{r}'\right)}\\ &= \sum_{\{p_{q_s}\}}\exp\left(j\sum_{\{q_s\}}p_{q_s}\phi_{q_s}\right)B_{\{q_{q_s}\}}^{MIMO}\underbrace{\sum_{m,n}\frac{\exp\left[j\sum_{q_s}p_{q_s}\Delta_{m,n}\left(r_q;r_s\right)-j\Delta_{nm}\left(r;\mathbf{r}'\right)\right)\right]}{R_{nm}(r)R_{nm}\left(\mathbf{r}'\right)}}_{A_{\{p_{q_s}\}}^{MIMO}\left(r,\mathbf{r}';\{p_{q_s}\}\right)}\\ &= \sum_{\{p_{q_s}\}}\exp\left(j\sum_{\{q_s\}}p_{q_s}\phi_{q_s}\right)\underbrace{A_{\{q_s\}}^{MI}\left(\boldsymbol{r},\mathbf{r}'\right)B_{\{p_s\}}^{MIMO}}_{A_{\{p_{q_s}\}}^{MIMO}\left(r,\mathbf{r}'\{\{q_s\}\right)}}\end{aligned}\tag{D3}$$

Now, the derivation of the MIMO's system response of the one-bit coding metasurface is completed, i.e.,

$$\begin{aligned}\widehat{\mathcal{H}}_{MIMO}\left(\boldsymbol{r},\mathbf{r}';\{q_s\}\right) &= \underbrace{E_{1\ \text{MIMO}}\ \left(\boldsymbol{r},\mathbf{r}';\{q_s\}\right)}_{\text{leading term}}\\ &+\underbrace{\sum_{\{p_{q_s}\}/\left\{\sum_{\{q_s\}}|p_{q_s}|=1\&p_{\ q_s\neq -1}\right\}}E_{\{q_s\}}^{MIMO}\left(\boldsymbol{r},\mathbf{r}';\{q_s\}\right)\exp\left[j\sum_{s=1}^{S}\sum_{q_s=1}^{Q_s}p_{q_s}\phi_{q_s}\right]}_{\text{perturbation terms}}\end{aligned}\tag{D4}$$

where $E_1^{MIMO}\left(\boldsymbol{r},\mathbf{r}';\{q_s\}\right)=B_1^{MIMO}\sum_{s=1}^{S}\sum_{q_s=1}^{Q_s}\exp\left(j\phi_{q_s}\right)A_1^{SISO}\left(\boldsymbol{r},\mathbf{r}';q,s\right)$. In addition, the operator $\sum_{\{p_{q_s}\}/\left\{\sum_{\{q_s\]}|p_{q_s}|=1\&p_{q_s}\neq -1\right\}}$ is defined similar to that of **Eq .C4**.

Discussion 1. Derivation of $B_{\{p_{qs}\}}^{MIMO}$ for the double-input double output case.

Here, we briefly discuss the calculation of $B_{\{p_{qs}\}}^{MIM}$ for a special case of S = 2 and $Q_1 = Q_1 = 1$. In this case, the closed-form solution of $B_{\{p_{q_s}\}}^{MIMO}$ can obtained:

$$B_{\{p_{qs}\}}^{MIMO}=\frac{-j^{(p_1+p_2+1)}}{\pi}\int_{-\infty}^{+\infty}\frac{J_{p_1}(\xi)J_{p_2}(\xi)}{\xi}d\xi=\begin{cases}0, & p_1+p_2\text{ is even}\\ \frac{-j(p_1+p_2+1)}{p_1+p_2}\cdot\left(\frac{2}{\pi}\right)^2\cdot\frac{\sin\left[\left(p_1-p_2\right)\frac{\pi}{2}\right]}{p_1-p_2}, & p_1+p_2\text{ is odd}\end{cases}$$

and $B_0^{MIMO}=\frac{2}{\pi}\int_0^{\infty}\frac{1}{\xi}J_0(\xi)J_1(\xi)d\xi=\left(\frac{2}{\pi}\right)^2$.

Discussion 2. Parasitic radiation beams of the one-bit coding metasurface

We provide some insights into the parasitic radiation beams when multiple sources and multiple intended receivers are deployed in the far-field region of the one-bit coding metasurface. Similarly, we treat $\sum_{s=1}^{S}\sum_{q_s=1}^{Q_s}p_{q_s}\Delta_{m,n}\left(\boldsymbol{r}_q;\boldsymbol{r}_s\right)-\Delta_{nm}\left(\boldsymbol{r};\boldsymbol{r}'\right)$ as follows:

$$\begin{aligned}\sum_{s=1}^{S}\sum_{q_s=1}^{Q_s}p_{q_s}\Delta_{m,n}\left(\boldsymbol{r}_q;\boldsymbol{r}_s\right)-\Delta_{nm}\left(\boldsymbol{r};\boldsymbol{r}'\right) &= -\frac{k}{2z}\underbrace{\left(1+\frac{z}{z'}-\sum_{s=1}^{S}\sum_{q_s=1}^{Q_s}p_{q_s}\left(\frac{z}{z_s}+\frac{z}{z_q}\right)\right)}_{\beta^{MIMO}}\rho_{mn}^2\\ &+\frac{k}{z}\underbrace{\left(\rho_x+\frac{z}{z'}\rho_x'-\sum_{s=1}^{S}\sum_{q_s=1}^{Q_s}p_{q_s}\left(\frac{z}{z_s}\rho_{sx}+\frac{z}{z_q}\rho_{qx}\right)\right)}_{b_x^{MIMO}}nd_x\\ &+\frac{k}{z}\underbrace{\left(\rho_y+\frac{z}{z'}\rho_y'-\sum_{s=1}^{S}\sum_{q_s=1}^{Q_s}p_{q_s}\left(\frac{z}{z_s}\rho_{sy}+\frac{z}{z_q}\rho_{qy}\right)\right)}_{b_x^{MIMO}}md_y+k\mathcal{E}^{MIMO}.\end{aligned}\tag{D5}$$

Herein, $\varepsilon^{MIMO}=p\left(z_s+z_q\right)-\left(z'+z\right)+\sum_{s=1}^{S}\sum_{q_s=1}^{Q_s}p_{q_s}\left(\frac{\rho_s^2}{2z_s}+\frac{\rho_q^2}{2z_q}\right)-\left(\frac{\rho'^2}{2z'}+\frac{\rho^2}{2z}\right)$. Then, the closed-form solution of $A_{\{p_{q_s}\}}^{MIMO}\left(\boldsymbol{r},\mathbf{r}',\{q_s\}\right)$ can be derived as:

$$\begin{aligned}A_{\{p_{q_s}\}}^{MIMO}\left(\boldsymbol{r},\boldsymbol{r}'\right) &= \sum_{m,n}\frac{\exp\left(j\left[\sum_{s=1}^{S}\Sigma_{q_s=1}^{Q_s}p_{\ q_s\Delta_{m,n}(r_q;\boldsymbol{r}_s)-\Delta_{m,n}(r;r')}\right]\right.}{R_{nm}(r)R_{nm}\left(r'\right)}\\ &\approx\frac{1}{zz\prime}\frac{\pi}{\alpha+i\frac{k\beta^{MIMO}}{2z}}\exp\left(-\frac{k^2}{4Z^2}\frac{\left(b_x^{MIMO}\right)^2+\left(b_y^{MIMO}\right)^2}{\alpha+i\frac{k\beta^{MIMO}}{2z}}\right)\exp\left(jk\varepsilon^{MIMO}\right).\end{aligned}\tag{D6}$$

From the above expression, we note that the parasitic radiation beams can be observed at $\left(\rho_x\left(\{p_{q_s}\}\right),\rho_y\left(\{p_{q_s}\}\right),z\right)$, where $\rho_x\left(\{p_{q_s}\}\right)=\sum_{s=1}^{S}\sum_{q_s=1}^{Q_s}p_{q_s}\left(\frac{z}{z_s}\rho_{sx}+\frac{z}{z_q}\rho_{qx}\right)-\frac{z}{z'}\rho_x'$, and $\rho_y\left(\{p_{q_s}\}\right)=\sum_{s=1}^{S}\sum_{q_s=1}^{Q_s}p_{q_s}\left(\frac{z}{z_s}\rho_{sy}+\frac{z}{z_q}\rho_{qy}\right)-\frac{z}{z'}\rho_y'$.

Discussion 3. Far-field solution of **Eq. D4**

We study the system response $\widehat{\mathcal{H}}_{\mathrm{MIMO}}$ when the source and intended receivers are in the far-field region of the metasurface. Similar to the SIMO case discussed in **Appendix C**, we deal with $A^{MIMO}_{\{q_s\}}\left(\boldsymbol{r},\mathbf{r}',\{q_s\}\right)$ as follows

$$\begin{aligned}
A^{MIO}_{\{q_{q_s}\}}\left(\boldsymbol{r},\boldsymbol{r}';\{q_s\},s\right) &\approx \frac{\exp\left[jk\sum_{q_s}p_{q_s}\left(r_{q_s}+r_s\right)-jk\left(\left(r+r'\right)\right)\right]}{rr'} \\
&\times\sum_{m,n}\exp\left[-jk\boldsymbol{r}_{m,n}\cdot\sum_{q_s}p_{q_s}\left(\hat{\boldsymbol{r}}_q+\hat{\boldsymbol{r}}_s\right)+jk\boldsymbol{r}_{m,n}\cdot\left(\hat{\boldsymbol{r}}+\hat{\boldsymbol{r}}'\right)\right] \\
&\approx -\frac{\exp\left[jk\sum_{q_s}p_{q_s}\left(r_q+r_s\right)-j\left(\left(r+r'\right)\right)\right]}{rr'} \\
&\times L_xL_y\,\mathrm{sinc}\left(\frac{1}{2}kL_x\xi^{MIMO}\left(\{q_s\}\right)\right)\mathrm{sinc}\left(\frac{1}{2}kL_y\eta^{MIMO}\left(\{q_s\}\right)\right)
\end{aligned} \tag{D7}$$

Herein, ξ^{MIMO} and η^{MIMO} are defined as:

$$\begin{aligned}
\xi^{MIMO}\left(\{p_{q_s}\}\right) &= \sin(\alpha)\cos(\beta)+\sin\left(\alpha'\right)\cos\left(\beta'\right) \\
&\quad-\sum_{q_s}p_{q_s}\left[\sin\left(\alpha_{q_s}\right)\cos\left(\beta_{q_s}\right)+\sin\left(\alpha_s\right)\cos\left(\beta_s\right)\right] \\
\eta^{MIMO}\left(\{p_{q_s}\}\right) &= \sin(\alpha)\sin(\beta)+\sin\left(\alpha'\right)\sin\left(\beta'\right) \\
&\quad-\sum_{q_s}p_{q_s}\left[\sin\left(\alpha_{q_s}\right)\sin\left(\beta_{q_s}\right)+\sin\left(\alpha_s\right)\sin\left(\beta_s\right)\right].
\end{aligned}$$

From **Eq. D7**, the parasitic radiation beam is observed when the vector of $\sum_{q_s}p_{q_s}\left(\hat{\boldsymbol{r}}_q+\hat{\boldsymbol{r}}_s\right)+\hat{\boldsymbol{r}}+\hat{\boldsymbol{r}}'$ is perpendicular to the normal of the one-bit coding metasurface.

Appendix E Derivation of Eq. 9

We here detail the derivation of **Eq. 9** in the main text. In terms of the definition of statistical coherence, we arrive at

$$\begin{aligned}
\left\langle\widehat{\mathcal{H}}_{SIMO}\left(\boldsymbol{r}_i\right),\widehat{\mathcal{H}}_{SIMO}\left(\boldsymbol{r}_j\right)\right\rangle &= \left|\mathrm{B}_0\right|^2\sum_{q=1}^{Q}\sum_{q'=1}^{Q}A_q\left(\boldsymbol{r}_i\right)A^*_{q'}\left(\boldsymbol{r}_j\right)\left\langle\exp\left(j\left(\phi_q-\phi_{qq'}\right)\right)\right\rangle \\
&+\mathrm{B}_0\sum_{q=1}^{Q}A_q\left(\boldsymbol{r}_i\right)\sum_{p_{i:1\to Q}}E^*_{\{p_i\}}\left(\boldsymbol{r}_j\right)\left\langle\exp\left[j\phi_q-j\sum_{q'=1}^{Q}p_{qq'}\phi_{q'}\right]\right\rangle \\
&+B^*_0\sum_{q=1}^{Q}A^*_q\left(\boldsymbol{r}_j\right)\sum_{p_{i:1\to Q}}E_{\{p_i\}}\left(\boldsymbol{r}_i\right)\left\langle\exp\left[j\sum_{qq'=1}^{Q}p_{qq'}\phi_{q'}-j\phi_q\right]\right\rangle \\
&+\sum_{p_{i:1\to Q}}\sum_{p'_i:1\to Q}E_{\{p_i\}}\left(\boldsymbol{r}_i\right)E^*_{\{p'_i\}}\left(\boldsymbol{r}_j\right)\left\langle\exp\left[j\sum_{q=1}^{Q}\left(p_q-p'_q\right)\phi_q\right]\right\rangle
\end{aligned} \tag{E1}$$

Taking the following identical equations into account, namely,

$$\begin{aligned}
&\left\langle\exp\left(j\left(\phi_q-\phi_{q'}\right)\right)\right\rangle=\delta_{q-q'}, \\
&\left\langle\exp\left[j\sum_{q'=1}^{Q}p_{q'}\phi_{q'}-j\phi_q\right]\right\rangle=\delta_{p_q-1-nM_q}\prod_{q'=1,q'\neq q}^{Q}\delta_{p_{q'}-nM_{q'}}, \\
&\left\langle\exp\left[j\sum_{q=1}^{Q}\left(p_q-p'_q\right)\phi_q\right]\right\rangle=\prod_{q=1}^{Q}\delta_{p_q-p'_q-nM_q},
\end{aligned}$$

we can rewrite **Eq. E1** as:

$$\begin{aligned}
\left\langle\widehat{\mathcal{H}}_{SIMO}\left(\boldsymbol{r}_i\right),\widehat{\mathcal{H}}_{SIMO}\left(\boldsymbol{r}_j\right)\right\rangle &= \left|\mathrm{B}_0\right|^2\sum_{q=1}^{Q}A_q\left(\boldsymbol{r}_i\right)A^*_q\left(\boldsymbol{r}_j\right) \\
&+\mathrm{B}_0\sum_{q=1}^{Q}A_q\left(\boldsymbol{r}_i\right)\sum_{n_{i:1\to Q/n}}E^*_{\{M_in_i\}}\left(\boldsymbol{r}_j\right) \\
&+B^*_0\sum_{q=1}^{Q}A^*_q\left(\boldsymbol{r}_j\right)\sum_{n_{i:1\to Q/n_q}}E_{\{M_in_i\}}\left(\boldsymbol{r}_i\right) \\
&+\sum_{p_{i:1\to Q}}\sum_{p'_i:1\to Q}E_{\{p_i\}}\left(\boldsymbol{r}_i\right)E^*_{\{p'_i\}}\left(\boldsymbol{r}_j\right)\prod_{q=1}^{Q}\delta_{p_q-p'_q-nM_q}
\end{aligned} \tag{E2}$$

Herein, we have introduced the following notation

$$\sum_{n_{i:1\to Q/n_q}}\equiv\sum_{n_1=-N,}^{N},\cdots\sum_{n_{q-1}=-N}^{N}\sum_{n_q=-N+1/M_q}^{N+1/M_q}\sum_{n_{q+1}=-N}^{P}\cdots\sum_{n_Q=-N}^{N}$$

We here consider a more realistic scenario that two receivers are well separated in terms of the Rayleigh limit, i.e., $|A_q(\boldsymbol{r}_i)| \approx 0$ for $i \neq q$. Then, **Eq. E2** reads:

$$\left\langle \widehat{\mathcal{H}}_{SIMO}(\boldsymbol{r}_i), \widehat{\mathcal{H}}_{SIMO}(\boldsymbol{r}_j) \right\rangle \approx \mathrm{B}_0 A_i(\boldsymbol{r}_i) \sum_{\frac{n_{i:1\to Q}}{n_q}} E^*_{\{M_i n_i\}}(\boldsymbol{r}_j) + B_0^* A_j^*(\boldsymbol{r}_j) \sum_{n_{i:1\to Q/n_q}} E_{\{M_i n_i\}}(\boldsymbol{r}_i), \quad \text{for } i \neq j$$

$$\left\langle \widehat{\mathcal{H}}_{SIMO}(\boldsymbol{r}_i), \widehat{\mathcal{H}}_{SIMO}(\boldsymbol{r}_i) \right\rangle = |\mathrm{B}_0 A_0|^2 + \mathrm{B}_0 A_i(\boldsymbol{r}_i) \sum_{n_{i:1\to Q/n_q}} E^*_{\{M_i n_i\}}(\boldsymbol{r}_j) + B_0^* A_i^*(\boldsymbol{r}_i) \sum_{n_{i:1\to Q/n_q}} E_{\{M_i n_i\}}(\boldsymbol{r}_i)$$

Now, the derivation of **Eq. 10** in the main text is completed.

Appendix F Derivation of Eq. 10

We provide briefly the derivation of **Eq. 10** in the main text. Along the same line as that in **Appendix E**, we can arrive at the expressions of μ_u^{SIMO} and σ_u^{SIMO}

$$\begin{aligned} \mu_u^{\mathrm{SIMO}} &= \left\langle \widehat{\mathcal{H}}_{SIMO}(\boldsymbol{r}_u, \boldsymbol{r}_s; \{q\}, s) \right\rangle \\ &= \mathrm{A}_0\ \mathrm{B}_0 \exp(j\phi_i) + \sum_{p_{i:1\to Q}} \left(E_{\{p_i\}}(\boldsymbol{r}_i) \exp[j p_i \phi_i] \prod_{q=1, q\neq i}^{Q} \delta_{p_q - nM_q} \right) \end{aligned} \tag{F1}$$

$$\begin{aligned} \sigma_u^{SIMO} &= \left\langle \left| \widehat{\mathcal{H}}_{SIMO}(\boldsymbol{r}_u, \boldsymbol{r}_s; \{q\}, s) - \left\langle \widehat{\mathcal{H}}_{SIMO}(\boldsymbol{r}_u, \boldsymbol{r}_s; \{q\}, s) \right\rangle \right|^2 \right\rangle \\ &= |\mathrm{B}_0|^2 \sum_{q=1, q\neq i}^{Q} \sigma_q^2 \lfloor A_q(\boldsymbol{r}_i) \rceil^2 + \chi(\{M_q\}), \end{aligned} \tag{F2}$$

in which,

$$\begin{aligned} \chi(\{M_q\}) &\equiv \sum_{\{p_{i/nM_i}\}} \sum_{\{p_i'/nM_i\}} E_{\{p_i\}}(\boldsymbol{r}_i) E^*_{\{p_i'\}}(\boldsymbol{r}_i) \exp\left[j(p_i - p_i')\phi_i\right] \prod_{q=1}^{Q} \delta_{p_q - p_q' - nM_q} \\ &\leqslant \sum_{\{p_{i/nM_i}\}} \sum_{\{p_i'/nM_i\}} \left| E_{\{p_i\}}(\boldsymbol{r}_i) E^*_{\{p_i'\}}(\boldsymbol{r}_i) \right| \prod_{q=1}^{Q} \delta_{p_q - p_q' - nM_q} \end{aligned} \tag{F3}$$

wherein

$$\sum_{\{p_i'/nM_i\}} \equiv \sum_{\substack{p_1=-P, \\ p_1\neq nM_1,}}^{P} \cdots \sum_{p_{q-1}=-P, p_{q-1}\neq nM_{q-1}}^{P} \sum_{p_q=-P}^{P} \sum_{p_{q+1}=-P, p_{q+1}\neq nM_{q+1}}^{P} \cdots \sum_{\substack{p_Q=-P. \\ p_Q\neq nM_Q}}^{P}$$

Appendix G Discussions on Fig. 3

In **Fig.H1(a)** and **H2(c)**, we report the dependence of $\Delta\varphi_{\mathrm{SISO}}(\boldsymbol{r}_q)$ on $\boldsymbol{r}_q$ for QPSK ($M_q = 4$) with the incident source deployed at $(0, 0, 2\ \mathrm{m})$ and $(0, 1.15\ \mathrm{m}, 2\ \mathrm{m})$, respectively. We note that the source is deployed in the near-field region of the metasurface. Correspondingly, the dependences of EC^{SISO} on $\boldsymbol{r}_q$ are also provided in **Fig. H1(b)** and **H2(d)**, respectively. It can be observed from this set of results that the one-bit coding metasurface has the ability to perform the QPSK information encoding with high fidelity within the whole observation region.

We next examine the ability of the one-bit coding metasurface to perform PSK information encoding by varying its scale. **Figure H2** shows the results for the case of 16-level PSK, where the simulation setup is the same as that in **Fig. 3c** in the main text. More specifically, **Figs. H2(b-d)** present the dependence of the half-power-beam-width (HPBW), the beam scanning error, and the ratio of the leading term to the perturbation terms of the radiation beam on the metasurface size for four selected locations $\boldsymbol{r}_q$ marked with (1) (2) (3) and (4) in **Fig. H2(a)**. From this set of figures, we observe that the performance of the one-bit coding metasurface in manipulating the beam and associated information can be efficiently improved by increasing the aperture of metasurface.

Appendix H Bit error analysis

We give the analysis on bit error rate (BER) for the one-bit coding metasurface. For discussion convenience, several notations are introduced. With loss of generality, we consider the wireless channel for transferring digital information with M-level phase shift key (MPSK) modulation, and use the Bayesian decision rule for information retrieval. With reference to Supplementary Figure S1, for the i th information symbol, the intended phase is μ_i, the biased mean phase is θ_i due to the one-bit quantization of the coding metasurface, and the total noise level (the conventional system noise plus the one-bit-quantization noise) is σ_i^2. Then, BER in total reads

$$BER = 1 - \sum_{i=1}^{M} \int_{2\pi(i-1)/M}^{2\pi i/M} \frac{1}{\sqrt{2\pi}\sigma_i} \exp\left(-\frac{(x - \theta_i - \mu_i)^2}{2\sigma_i^2} \right) dx \tag{H1}$$

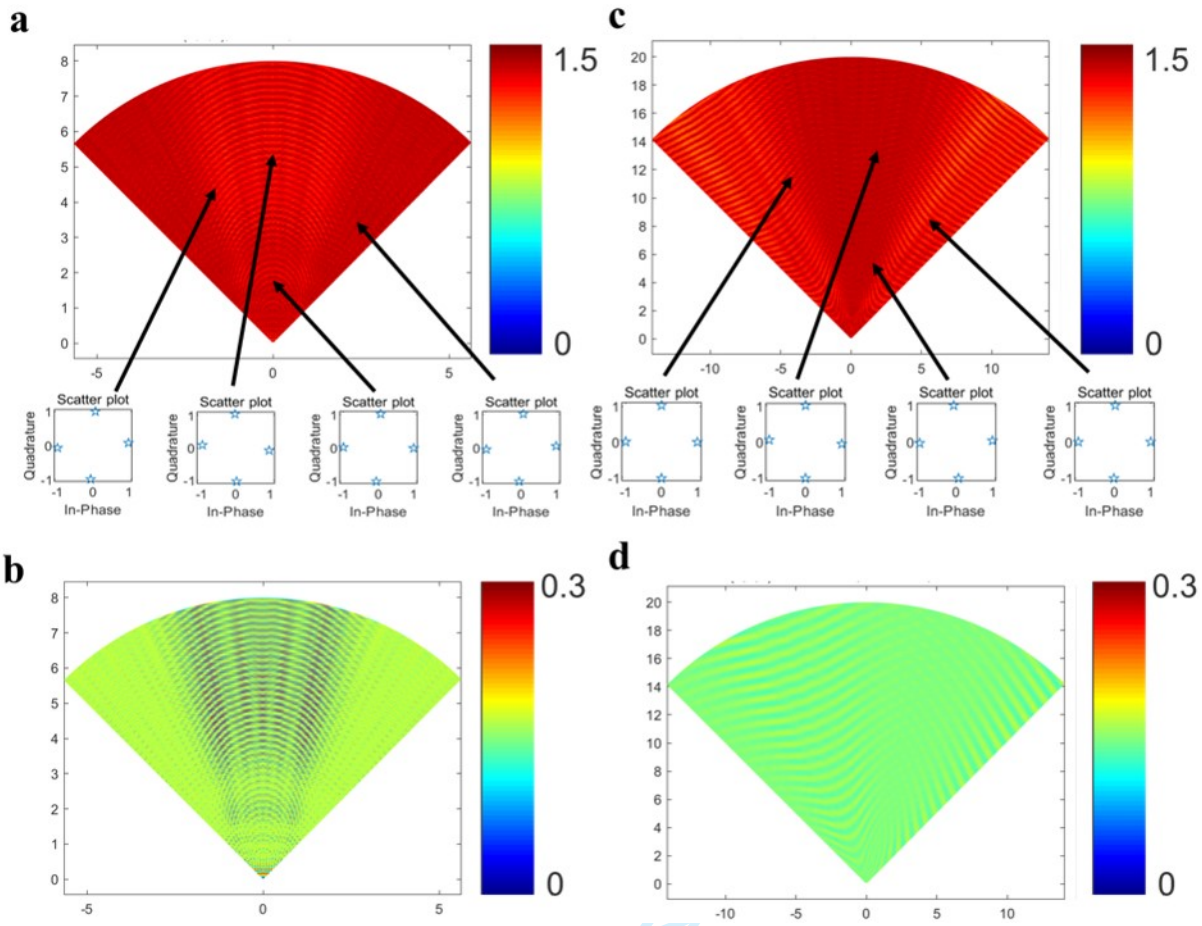

Figure H1 QPSK with the one-bit coding metasurface in SISO when the source is deployed in the near-field region of the metasurface. **a,c.** Dependence of phase resolution $\Delta\varphi_{\rm SISO}$ on the receiver's location $\boldsymbol{r}_q$. Considered receiver locations are within a distance between 0 and 20 m from the metasurface for azimuth between -60° and 60°. The insets provide representative constellation diagrams. Different levels of PSK and source locations are considered, as indicated in the subfigure titles. The source is deployed at $(0, 0, 2$ m) in **a**, while $(0, 1.3$ m$, 2$ m) in **c**. **b,d.** Dependence of $EC^{\rm SISO}$ on $\boldsymbol{r}_q$ for the same settings as in **a** and **c**.

Figure 7 in the main text shows the dependence of BER on M with system SNR of 20 dB, where the source and receiver are deployed in the near-field region of the one-bit coding metasurface. As a compliment, we consider the performance of the one-bit coding metasurface when the source and receiver are in its far-field region. Figure A6 compares BERs of the one-bit and continuous coding metasurfaces as a function of phase quantization levels in the SISO setting, where the source and receiver are located at $(0, 0, 1$ km) and $(0, 0, 2$ km), respectively. **Fig. H3(a)** shows the dependence of BER on the phase quantization level M in a system with SNR of 20 dB, while **Figs.H3(b)** and **H3(c)** report the constellation diagrams of four-level PSK information phase quantization levels for the continuous and one-bit coding metasurfaces, respectively. The axes are normalized by $B_0^{\rm SIMO}$. The red-marked and black-marked stars of the constellation diagrams in b and **c** correspond to the system-noise-free case. Notice that the M-PSK ($M > 2$) digital information is degraded to 2-PSK when the one-bit coding metasurface is used. That is to say, the one-bit coding metasurface fails to manipulate the EM information with high-order PSK when the receiver and source are in the blind district.

Appendix I Discussions about non-ideal one-bit quantization of programmable coding metasurfaces

We discuss the system response of the coding metasurface with non-ideal one-bit quantization. Particularly, when the meta-atom is illuminated by a plane wave, its binary response states read:

$$f(x) = \begin{cases} A_+ e^{j\phi_+}, & \text{for state } '1' \\ A_- e^{j\phi_-}, & \text{for state } 0' \end{cases}, \tag{I1}$$

where $0 \leqslant A_+, A_- \leqslant 1$, and $0 \leqslant \phi_+, \phi_- < 2\pi$. Recall the step function denoted by $u(x) = \begin{cases} 1, & x > 0 \\ \frac{1}{2}, & x = 0, \\ 0, & x < 0 \end{cases}$, then the above piece-wise function is expressed as:

$$f(x) = A_+ e^{j\phi_+} u(x) + A_- e^{j\phi_-} u(-x) \tag{I2}$$

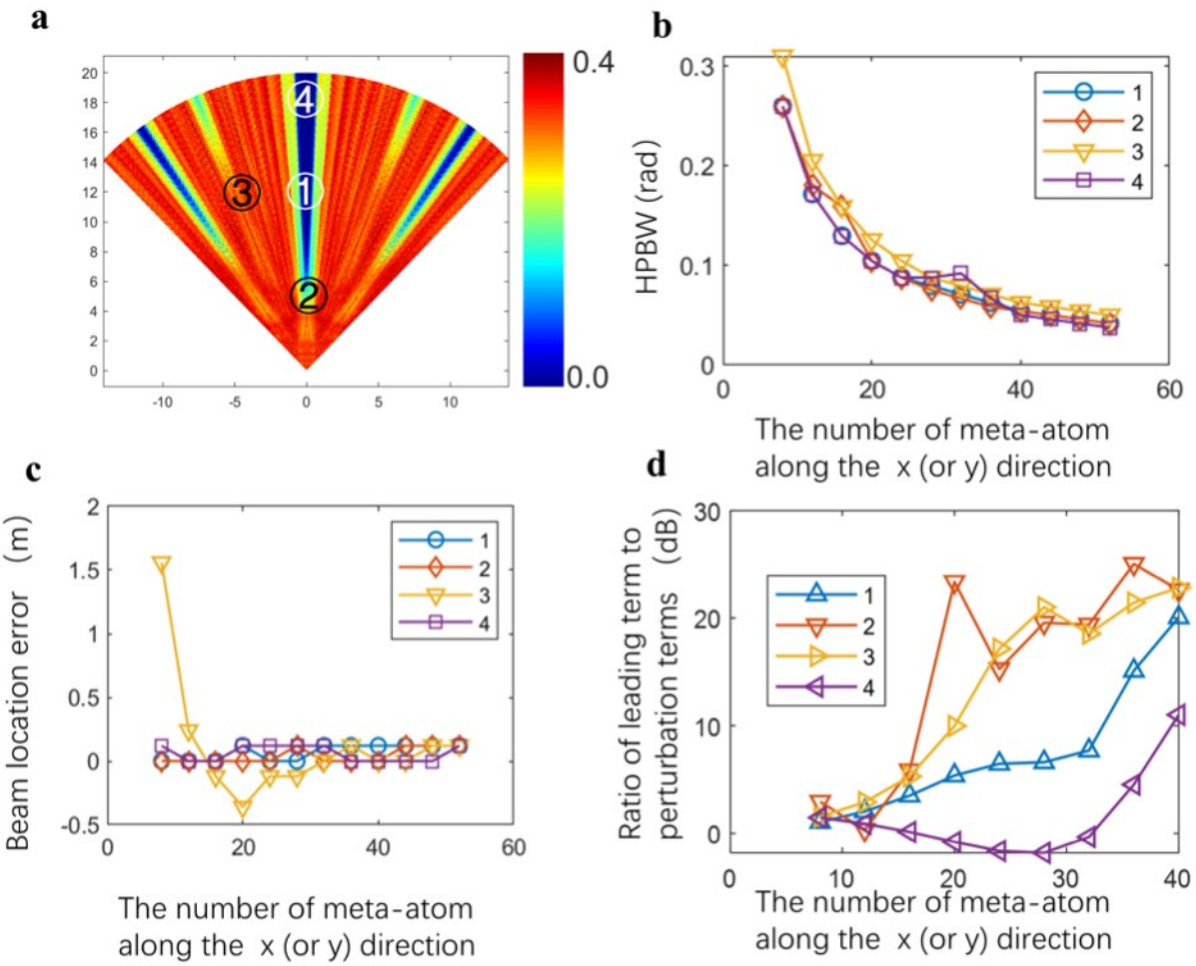

Figure H2 16-level PSK with a one-bit coding metasurface in SISO, where the source is deployed at $(\mathbf{0}, \mathbf{0}, \mathbf{2km})$. **a**. Dependence of phase resolution $\Delta\varphi_{\mathrm{SISO}}$ on the receiver's location $\boldsymbol{r}_q$. Considered receiver locations are within a distance between 0 and 20 m from the metasurface for azimuth between -60° and 60°. **b-d**. Dependence of HPBW, beam scanning error, and ratio of the leading term to the perturbation terms of the radiation beam on the metasurface size for four locations $\boldsymbol{r}_q$ marked with (1) (2) (3) and (4) in **Fig. H2(a)**, respectively.

Immediately, **Eq. I2** can be further expressed as

$$\begin{aligned} f(x) &= \frac{\left(A_+ e^{j\phi_+ + A_- e^{j\phi_-}}\right)}{2} + \frac{\left(A_+ e^{j\phi_+ - A_- e^{j\phi_-}}\right) e^{-j\pi/2}}{2\pi} \int_{-\infty}^{\infty} \frac{\exp(jx\xi)}{\xi} d\xi \\ &= \frac{\left(A_+ e^{j\phi_+ + A_- e^{j\phi_-}}\right)}{2} + \frac{\left(A_+ e^{j\phi_+ - A_- e^{j\phi_-}}\right)}{2} \cdot \frac{-j}{\pi} \int_{-\infty}^{\infty} \frac{\exp(jx\xi)}{\xi} d\xi \end{aligned} \tag{I3}$$

It is clear that we have established a simple relation of the responses between the ideal one-bit meta-atom and non-ideal meta-atom. As a result, for the non-ideal one-bit coding metasurface, its control coding patterns for SISO, SIMO and MIMO can be derived as:

$$\mathcal{C}_{m,n}^{\text{non-ideal,SISO}} = \gamma_0 + \gamma_1 \mathcal{C}_{m,n}^{SISO}, \tag{I4a}$$

$$\mathcal{C}_{m,n}^{\text{non-ideal,SIMO}} = \gamma_0 + \gamma_1 \mathcal{C}_{m,n}^{SIMO}, \tag{I4b}$$

$$\mathcal{C}_{m,n}^{\text{non-ideal,MIMO}} = \gamma_0 + \gamma_1 \mathcal{C}_{m,n}^{MIMO}. \tag{I4c}$$

For SISO, SIMO and MIMO, the system responses of the coding metasurface with the non-ideal one-bit quantization can be readily derived as:

$$\widehat{\mathcal{H}}_{\text{SISO}}^{\text{non-idea}} \left(\mathbf{r}, \mathbf{r}'; q, s\right) = \gamma_0 \sum_{m,n} \frac{\exp\left[-jk\Delta_{nm}\left(r; \mathbf{r}'\right)\right]}{R_{nm}(r) R_{nm}\left(\mathbf{r}'\right)} + \gamma_1 \widehat{\mathcal{H}}_{\text{SISO}} \left(\mathbf{r}, \mathbf{r}'; q, s\right), \tag{I5a}$$

$$\widehat{\mathcal{H}}_{\text{SIMO}}^{\text{non-ideal}} \left(\mathbf{r}, \mathbf{r}'; \{q\}, s\right) = \gamma_0 \sum_{m,n} \frac{\exp\left[-jk\Delta_{nm}\left(\boldsymbol{r}; \mathbf{r}'\right)\right]}{R_{nm}(r) R_{nm}\left(\mathbf{r}'\right)} + \gamma_1 \widehat{\mathcal{H}}_{\text{SIMO}} \left(\mathbf{r}, \mathbf{r}'; \{q\}, s\right), \tag{I5b}$$

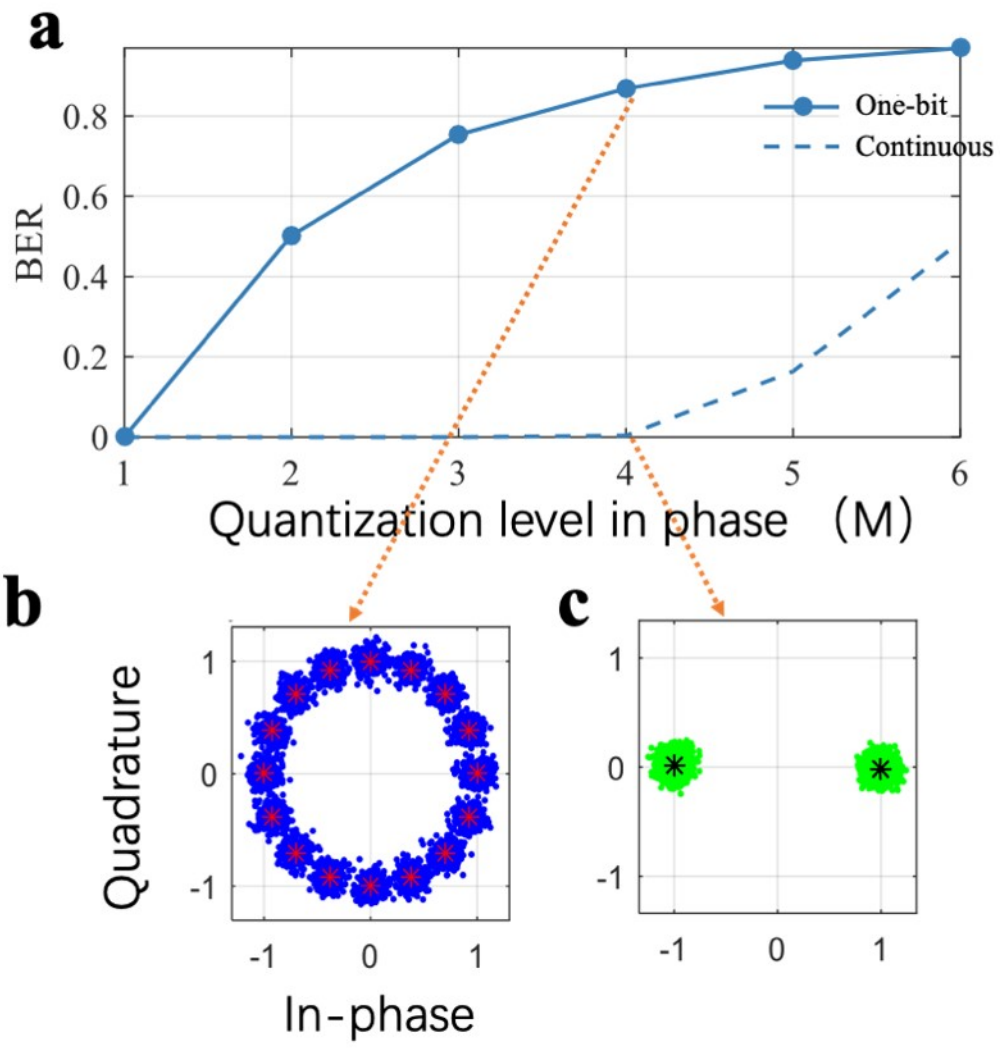

Figure H3 BER comparison of the one-bit and continuous metasurfaces in the SISO setting. **a**. Dependence of BER on the phase quantization level M in a system with SNR of 20 dB, in which the receiver and source are in the "blind district" of the metasurface. The solid and dashed lines represent the cases of continuous and one-bit coding metasurfaces. **b,c**. Constellation diagrams of the 4-PSK phase quantization levels for the continuous and one-bit coding metasurfaces, respectively. The axes are normalized by B_0^{SIMO} . The red-marked and black-marked stars of the constellation diagrams in **b** and **c** correspond to the system-noise-free case.

$$\widehat{\mathcal{H}}_{\mathrm{MIMO}}^{\text{non-ideal}}\left(\mathbf{r},\mathbf{r}';\{q_s\}\right)=\gamma_0\sum_{m,n}\frac{\exp\left[-j\Delta_{nm}\left(r;\mathbf{r}'\right)\right]}{R_{nm}(r)R_{nm}\left(\mathbf{r}'\right)}+\gamma_1\widehat{\mathcal{H}}_{\mathrm{MIMO}}\left(\mathbf{r},\mathbf{r}';\{q_s\}\right). \tag{I5c}$$

We note that the term $\sum_{m,n}\frac{\exp[-j\Delta_{nm}(r;\mathbf{r}')]}{R_{nm}(r)R_{nm}(\mathbf{r}')}$ characterizes exactly the conventional Snell's reflection, where the metasurface serves as a perfectly planar reflection mirror. To see it more clearly, we consider the far-field approximation

$$\sum_{m,n}\frac{\exp\left[-jk\Delta_{nm}\left(r;\mathbf{r}'\right)\right]}{R_{nm}(r)R_{nm}\left(\mathbf{r}'\right)}\approx\frac{\exp\left(-jk\left(r+r'\right)\right)}{rr'}\sum_{m,n}\exp\left[jk\boldsymbol{r}_{m,n}\cdot\left(\hat{\boldsymbol{r}}+\hat{\boldsymbol{r}}'\right)\right)\Bigg] \tag{I6}$$

where the following far-field approximation is used:

$$\Delta_{m,n}\left(\boldsymbol{r};\mathbf{r}'\right)=k\left(\left|\mathbf{r}'-\boldsymbol{r}_{m,n}\right|+\left|\boldsymbol{r}-\boldsymbol{r}_{m,n}\right|\right)\approx k\left(r+r'-\boldsymbol{r}_{m,n}\cdot\left(\hat{\boldsymbol{r}}+\hat{\boldsymbol{r}}'\right)\right)$$

Now, it is clear that the term of $\sum_{m,n}\frac{\exp[-jk\Delta_{nm}(r;\mathbf{r}')]}{R_{nm}(r)R_{nm}(\mathbf{r}')}$ has a single radiation peak as $\hat{\boldsymbol{r}}=-\hat{\boldsymbol{r}}'$, i.e., the receiver is located in the mirror direction of the source with respect to the normal direction of metasurface. That is to say, the non-ideal one-bit quantization will give rise to the radiation leakage in the mirror direction of the source with respect to the metasurface normal.

Figure H4 shows the dependence of the beam's intensity on the choice of $(\Gamma,\Delta\theta)$ in SISO, where the source is deployed at the location of $(0,0,2$ m), and the map has been normalized with its maximum. Here, Γ and $\Delta\theta$ are defined as: $\Gamma=|A_+|/|A_-|$,

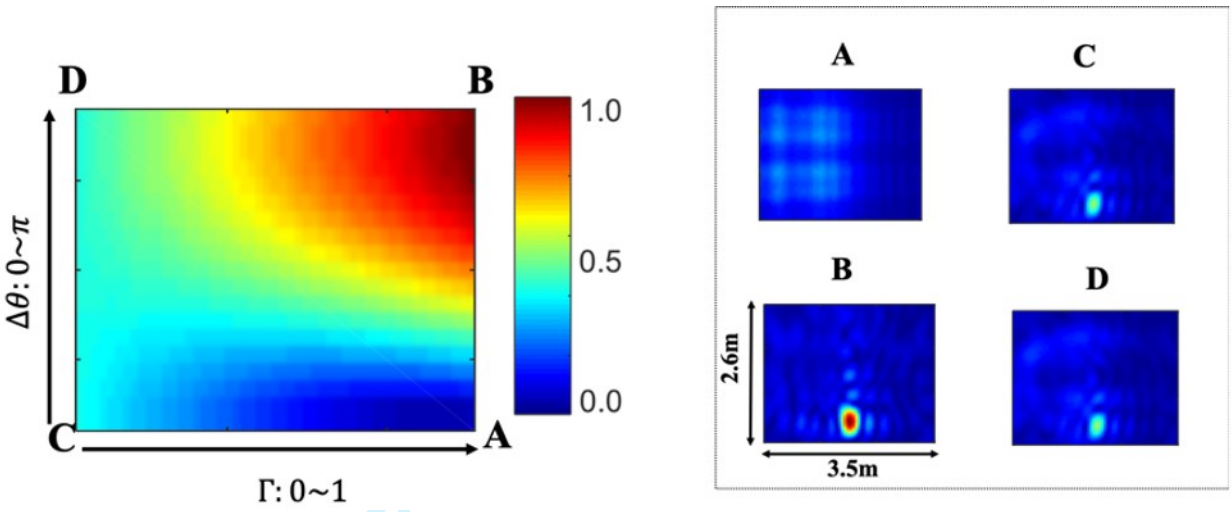

Figure H4 **Figure A7**. Dependence of the beam's intensity on the choice of $(\Gamma, \Delta\theta)$ in SISO. The left: the dependence of beam's intensity on the choice of $(\Gamma, \Delta\theta)$, in which the map has been normalized with its maximum. The right: spatial maps of $\left|\widehat{\mathcal{H}}_{SISO}^{\text{non-ideal}}\right|$ for four selected cases (A: $\Gamma = 1,\ \Delta\theta = 0$; B : $\Gamma = 1, \Delta\theta = \pi$; C : $\Gamma = 0, \Delta\theta = \pi$; D : $\Gamma = 0, \Delta\theta = \pi$) marked in the left figure, in which the source is located at $(0, 0, 2$ m) and the observation plane is at the distance of 3 m away from the metasurface.

and $\Delta\theta = \phi_+ - \phi_-$. In addition, we make the assumptions that $|A_-| = 1$ and $\phi_- = 0$. The spatial maps of $\left|\widehat{\mathcal{H}}_{SISO}^{\text{non-ideal}}\right|$ for four representative cases marked in the left of **Fig. H4** are shown in the right of **Fig. H4**. We clearly observe that the one-bit coding metasurface is robust to the non-ideal meta-atoms, in spite of some degraded performance more or less.